INORGANIC CHEMISTRY FRONTIERS

CCS 中国化学会 CHINESE CHEMICAL SOCIETY

ROYAL SOCIETY OF CHEMISTRY

Photonic materials derived from the [closo-B10H10]2- anion: Tuning photophysical properties in [closo-B10H8-1-X-10-(4-Y-NC5H5)]-

Journal:	*Inorganic Chemistry Frontiers*
Manuscript ID	QI-RES-11-2020-001353.R1
Article Type:	Research Article
Date Submitted by the Author:	03-Dec-2020
Complete List of Authors:	Kaszynski, Piotr; CBMM Polish Academy of Sciences, Heteroorganic Chemistry; Middle Tennessee State University, Chemistry; Uniwersytet Lodzki, Chemistry Kapuscinski, Szymon; Middle Tennessee State University, Chemistry; Uniwersytet Lodzki, Chemistry Abdulmojeed, Mustapha; Middle Tennessee State University, Chemistry Schafer, Tegan; Middle Tennessee State University, Chemistry Pietrzak, Anna; Lodz University of Technology, Chemistry; Middle Tennessee State University, Chemistry Hietsoi, Oleksandr; Middle Tennessee State University, Chemistry Friedli, Andrienne; Middle Tennessee State University, Chemistry

ARTICLE

Received 13th March 2020,
Accepted 00th January 20xx

DOI: 10.1039/x0xx00000x

Photonic materials derived from the [*closo*-$B_{10}H_{10}$]$^{2-}$ anion: Tuning photophysical properties in [*closo*-$B_{10}H_8$-1-X-10-(4-Y-NC_5H_5)]$^-$

Szymon Kapuściński,[a,b] Mustapha Abdulmojeed,[a] Tegan Schafer,[a] Anna Pietrzak,[a,c] Oleksandr Hietsoi,[a] Andrienne C. Friedli,*[a] and Piotr Kaszyński*[a,b,d]

The parent pyridine [*closo*-$B_{10}H_9$-1-NC_5H_5]$^-$ was substituted either at the antipodal B(10) position with CN, OAc, N_3, I, Br, SCN, pyridine, OEt, and morpholine, or at the C(4) position of the pyridine ring with CN, COOEt, Me, and OMe groups. The substituent effects on electronic absorption and emission properties, and also on the boron cage geometry were investigated experimentally and with DFT (B3LYP/Def2TZVP) computational methods. Experimental and theoretical results were correlated with Hammett σ_p parameters. Fluorescence was also investigated in the solid state and from aggregates (AIE). Solvent effects on photophysical properties of [*closo*-$B_{10}H_9$-1-NC_5H_5]$^-$ were correlated with E_T30 parameters, giving a slope of 0.71 for absorption and 0.17 for emission. Results demonstrated the substantial impact of the B(10) substituent on the HOMO and the C(4) substituent on the LUMO of the derivatives, which allows variation of the energy of the (π,π*) intramolecular charge transfer band in the range of 330–450 nm, and the emission energy in the range of 530–580 nm in MeCN solutions. The substituent effect on excitation energy is 2.4 times greater for substitution at the pyridine ring (LUMO control) than for the B(10) position (HOMO control). Additivity of the substituent effect was tested on [*closo*-$B_{10}H_8$-1-(NC_5H_4CN)-10-OEt]$^-$ with λ_{max} = 501.5 nm in MeCN and 560 nm in THF. These studies indicate that a substantial degree of control over photophysical properties is possible in derivatives of [*closo*-$B_{10}H_{10}$]$^{2-}$ through a combination of substituent and solvent (medium) effects.

Introduction

Photophysical properties of boron cluster derivatives continue to attract interest driven by fundamental science and applications in photonics and molecular electronics.[1-5] They have also been explored as potential NLO materials.[6-15] Current attention is focused on the *closo*-1,2-$C_2B_{10}H_{12}$ cluster (*ortho*-carborane), which acts as an effective enhancer of luminescent properties (both fluorescence and phosphorescence) of organic materials particularly in the solid-state[3] and in aggregates (*e.g.* aggregate induced emission, AIE).[4,16] Photophysical properties of other clusters are rarely described in the literature.

Parent *closo*-boranes are poor chromophores due to their typically large HOMO–LUMO gaps, and, consequently, they exhibit only weak absorptions above 200 nm. Substitution of the clusters with either electron-rich groups (in carboranes) or electron-poor groups (in *closo*-borane anions) leads to the appearance of intense low energy photo-induced intramolecular charge transfer (CT) bands, and often fluorescence. This strategy is particularly effective in π-zwitterionic derivatives of *closo*-borate anions, such as [*closo*-$B_{12}H_{12}$]$^{2-}$,[17-19] [*closo*-$B_{10}H_{10}$]$^{2-}$,[8,17,18] [*closo*-1-$CB_{11}H_{12}$]$^-$,[13, 20, 21] and [*closo*-1-CB_9H_{10}]$^-$,[21-23] in which the relatively high-lying HOMO is localized on the *closo*-borate anion and the LUMO is on the π onium fragment. For example, the CT process in tropylium (ousenes)[13,17,24,25] and pyridinium[8,18-23,26] zwitterions involves a (π,π*) excitation (HOMO–LUMO transition), which is schematically shown in Fig. 1. Relaxation of the excited state in the latter group of zwitterions also involves fluorescence with quantum yields up to 37%.[8, 19]

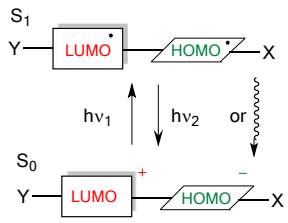

Fig. 1. Schematic representation of (π,π*) excitation and relaxation processes in π-zwitterionic derivatives of *closo*-boranes.

[a] Department of Chemistry, Middle Tennessee State University, Murfreesboro, TN 37130, USA
[b] Faculty of Chemistry, University of Łódź, Tamka 12, 91-403 Łódź, Poland
[c] Faculty of Chemistry, Łódź University of Technology, Żeromskiego 116, 90-924 Łódź, Poland
[d] Centre of Molecular and Macromolecular Studies, Polish Academy of Sciences, 90-363 Łódź, Poland

†Electronic Supplementary Information (ESI) available: full synthetic and compounds characterization details, NMR spectra, XRD, UV-vis, and computational details. See DOI: 10.1039/x0xx00000x

The 10-vertex dianion [*closo*-$B_{10}H_{10}$]$^{2-}$ (**A**, Fig. 2)[27, 28] is exceptional among *closo*-boranes: its D_{4d} symmetry allows for efficient interactions with π substituents,[29, 30] while the particularly high-lying HOMO[31] allows relatively low energy (π,π*) excitations in its zwitterionic derivatives. This is evident in [*closo*-$B_{10}H_9$-1-NC_5H_5]$^-$ (**1a**):[32] the CT band at 364.5 nm (3.39 eV, *log* ε = 3.85)[18] has the lowest energy among analogous derivatives of *closo*-borane anions,[18, 20, 22, 23] and extends into the visible range. Moreover, pyridinium derivatives of cluster **A** are photoluminescent in the visible range with a quantum yield up to 7% and Stokes shifts of about 1.4 eV.[8] Such compounds are of potential interest as photonic materials, especially if the absorption/emission energies can be tuned with substituents. To probe the extent of tunability of the excitations and emission energies in **1a**, we focused on a series of pyridinium derivatives **1** and **2** (Fig. 2), which are accessible through the recently discovered[32] selective functionalization of the apical positions in **A**.

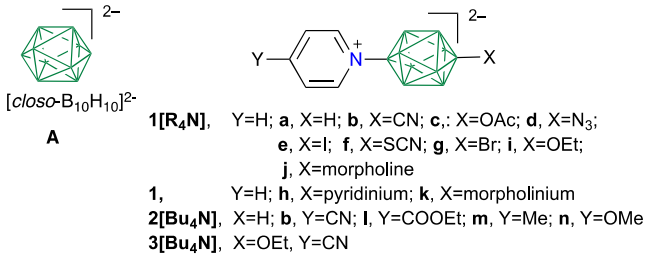

Fig. 2. Structures of dianion [*closo*-$B_{10}H_{10}$]$^{2-}$ (**A**) and pyridinium derivatives **1–3**. Each unsubstituted vertex corresponds to a B–H group.

Herein we report two series of pyridinium derivatives, **1** and **2**, that contain a range of substituents either at the B(10) apex of the cluster or at the C(4) position of the pyridine ring, respectively. Substituent effects were investigated in the two series with structural (XRD), spectroscopic, and DFT methods. Photophysical properties were measured in MeCN solutions and in the solid state, while aggregation effects on emission were examined for two selected derivatives in the MeCN/H_2O mixtures. Solvent effects on the position and intensity of the CT band were studied for the prototype [*closo*-$B_{10}H_9$-1-NC_5H_5]$^-$ (**1a**). Experimental data are augmented with DFT calculations, compared with theoretical geometry and excitation energies, and correlated with solvent and Hammett substituent parameters. Additivity of the substituent effects was tested on derivative [*closo*-$B_{10}H_8$-1-(NC_5H_4CN)-10-OEt]$^-$ (**3**).

Results

Synthesis

Our previous work demonstrated that monoiodonium [*closo*-$B_{10}H_9$-1-IPh]$^-$ (**4[Et$_4$N]**) undergoes nucleophilic substitution with pyridine to give **1a[Et$_4$N]** and it also reacts with the CN^- anion giving [*closo*-$B_{10}H_9$-1-CN]$^{2-}$ (**5b[Et$_4$N]**) in good yields.[32] This suggests a 3-step method for the preparation of series **1** through the intermediate [*closo*-$B_{10}H_8$-1-IPh-10-X]$^-$ (**6**, method A in Fig. 3). We also demonstrated that the reaction of bisiodonium [*closo*-$B_{10}H_8$-1,10-2(IPh)] (**7**) with AcO^- gives monosubstituted product **6c** with high selectivity,[32] which indicates an alternative two-step process leading to **1** (method B, Fig. 3). Access to phenyliodonium derivative [*closo*-$B_{10}H_8$-1-IPh-10-NC_5H_5] (**8**) would provide a third method (method C, Fig. 3) to obtain products **1**. Here we explore all three methods for preparation of pyridinium derivatives **1**.

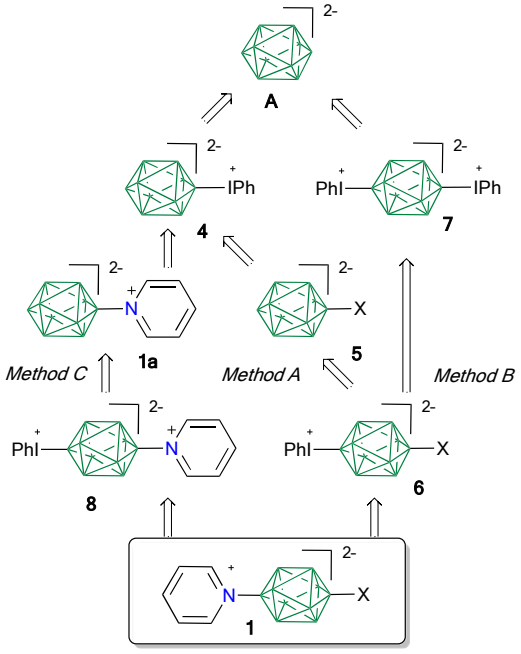

Fig. 3. Three synthetic approaches to the preparation of series **1**.

The initial synthesis of series **1** focused on the three-step method using **4[Bu$_4$N]**, which is more readily available than the **4[Et$_4$N]** salt.[33] To determine the scope of the method, the reactivity of **4[Bu$_4$N]** with several nucleophiles in MeCN at 60 °C was screened in NMR tube reactions. The progress of each reaction was monitored with ^{11}B NMR spectroscopy as the rate of disappearance of the starting anion **4**. Results demonstrated that the reactivity follows the order N_3^- > CN^- > Br > SCN^- > AcO^- >> morpholine. It was noted that only the N_3^- anion gave a single product, [*closo*-$B_{10}H_9$-1-N_3]$^{2-}$ (**5d**). The reaction of **4** with the CN^- anion was slower and the expected product was contaminated with a side product resulting from independent decomposition of **4** (complete decomposition after 16 hr in MeCN at 55-60 °C in the absence of any nucleophile). Other nucleophiles, SCN^-, AcO^-, morpholine, pyridine, Br^- and I^-, gave complex mixtures of products in which the desired product was either a minor component, or was not formed at all (pyridine, morpholine, Br^-, and I^-). Consequently, only the preparation of products **1b** and **1d** appear to be practical with method A.

Anion **5b** was obtained using a modification of our literature procedure[32] (Scheme 1). Thus, the reaction of **4[Bu$_4$N]** with $[Bu_4N]^+CN^-$ at 55 °C in MeCN gave a crude product containing about 60–65% of the expected **5b** and some unknown side products, from which pure **5b[Bu$_4$N]** was isolated in 50–55% yield by column chromatography followed

by recrystallization. The subsequent reaction of **5b[Bu$_4$N]** with PhI(OAc)$_2$ in MeCN solutions gave **6b[Bu$_4$N]**, which after purification with column chromatography was reacted with excess pyridine to give the expected product **1b[Bu$_4$N]** (Scheme 2). Synthesis of azide **1d[Bu$_4$N]** was more straightforward. Thus, **4[Bu$_4$N]** was smoothly reacted with 1.1 eq of [Bu$_4$N]$^+$N$_3^-$ and the resulting azide **5d[Nu$_4$N]** was isolated by column chromatography in 95% yield (Scheme 1). The azide subsequently converted to phenyliodonium **6d[Bu$_4$N]** and reacted with pyridine to give **1d[Bu$_4$N]** in 55% yield for the two-step process (Scheme 2).

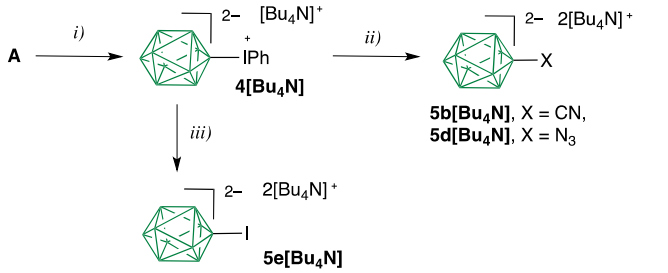

Scheme 1. Synthesis of intermediates **5**. *Reagents and conditions*: *i*) 30% aqueous AcOH, PhI(OAc)$_2$, [Bu$_4$N]$^+$[HSO$_4^-$], 0 ^{o}C, 1 h, 50%, ref.[33] ; *ii*) [Bu$_4$N]$^+$X$^-$, MeCN, 55 ^{o}C, 16 h, 50 - 95%; *iii*) *n*-BuLi, THF, [Bu$_4$N]$^+$[HSO$_4^-$], -10 to -5 ^{o}C, 1 h, 91%, ref.[33].

Iodo derivative **1e[Bu$_4$N]** was obtained in 38% overall yield by reacting iodide **5e[Bu$_4$N]**, obtained from **4[Bu$_4$N]** according to the literature method (Scheme 1),[33] with PhI(OAc)$_2$ in MeCN followed by reaction of the resulting [*closo*-B$_{10}$H$_8$-1-I-10-IPh]$^-$ (**6e[Bu$_4$N]**) with pyridine (Scheme 2). An alternative method of obtaining **6e[Bu$_4$N]** directly from bisiodonium **7** (method B) with controlled amounts of BuLi was much less efficient, and the desired product was isolated in 25% yield from a complex mixture of products using column chromatography. To facilitate crystal growth for XRD analyses, the cation in **1e[Bu$_4$N]** and in **1b[Bu$_4$N]** was exchanged for [Et$_4$N]$^+$ using Dowex-50 exchange resin followed by treatment of the eluent with [Et$_4$N]$^+$OH$^-$.

The preparation of acetoxy, thiocyanato, and bromo derivatives (**1c[Et$_4$N]**, **1f[Et$_4$N]** and **1g[Et$_4$N]**) was accomplished using bisiodonium derivative **7** according to method B (Fig. 3). Thus, acetate **6c[Et$_4$N]**, prepared as described before from **7**,[32] was reacted with excess pyridine to yield the desired product **1c[Et$_4$N]** in 74% yield. A similar reaction of **7** with 1.5 eq of [Et$_4$N]$^+$SCN$^-$ in MeCN at 60 ^{o}C gave a mixture of products, from which **6f[Et$_4$N]** was isolated by column chromatography in 16% yield. The subsequent thermolysis of **6f[Et$_4$N]** in pyridine solutions gave **1f[Et$_4$N]** in 78% yield. Bromide **1g[Et$_4$N]** was obtained in 56% overall yield from **7** in the same two step sequence reaction with 75% yield for each **6g[Et$_4$N]** and **1g[Et$_4$N]**.

Finally, dipyridinium derivative [*closo*-B$_{10}$H$_8$-1,10-2(NC$_5$H$_5$)] (**1h**) was obtained directly from bisiodonium **7** upon reaction with neat pyridine.

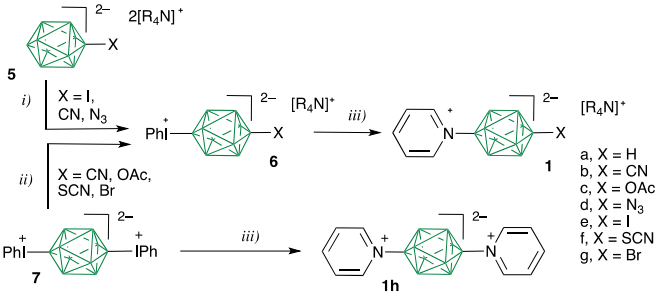

Scheme 2. Preparation of **1** using methods A and B. *Reagents and conditions*: *i*) PhI(OAc)$_2$, MeCN, 0 ^{o}C to r.t., 66-91%; *ii*) [R$_4$N]$^+$Nu$^-$, MeCN or THF or mixture, 55 ^{o}C, 16 h, 16-75%; *iii*) pyridine, 80 ^{o}C, 16 h, 48-83%

In an attempt to simplify the preparation of **1b[Bu$_4$N]**, bisiodonium **7** was reacted with 1.1 eq of the [Bu$_4$N]$^+$CN$^-$ in MeCN at 55 ^{o}C. The resulting mixture contained the desired **6b[Bu$_4$N]** as the main component, which was isolated by column chromatography in 53% yield. This process turned out to be more convenient than method A, although poor solubility of bisiodonium **7** in the reaction medium complicated the reaction progress and product isolation.

Method B was also tested as one-pot preparation of the azide **1d[Bu$_4$N]** and bromide **1g[Et$_4$N]** without purification of the intermediate monoiodonium derivatives **6d** and **6g**. In this case the final products were obtained in 64% (**1d[Bu$_4$N]**), and 68% (**1g[Et$_4$N]**) overall yields based on bisiodonium **7**.

Results with **4** and **7** indicate that the presence of an onium substituent in the antipodal position facilitates substitution of the PhI group in derivatives of **A**. In an effort to improve the yield for preparation of the thiocyanato derivative **1f[Et$_4$N]**, pyridinium derivative **8** was obtained by phenyliodination of **1a[Bu$_4$N]** in MeCN and isolated in 69% yield (method C, Scheme 3). The subsequent reaction of **8** with [Et$_4$N]$^+$SCN$^-$ in MeCN gave relatively clean conversion to product **1f[Et$_4$N]**, which was isolated in 55% yield.

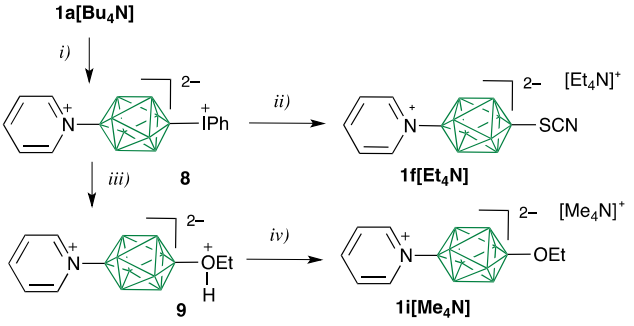

Scheme 3. Preparation of **1f** and **1i** using method C. *Reagents and conditions*: *i*) PhI(OAc)$_2$, MeCN, rt, 16 hr, 69%; *ii*) [Et$_4$N]$^+$SCN$^-$, MeCN, 80 ^{o}C, 16 h, 55%; *iii*) EtOH, 110 ^{o}C, 2.5 d, 69%; *iv*) MeCN, [Me$_4$N]$^+$OH$^-$ •5H$_2$O, 15 min, rt, 53%.

The demonstrated high reactivity of **8** towards SCN$^-$ suggests the possibility of its reaction with other nucleophiles even as weak as EtOH to obtain anion [*closo*-B$_{10}$H$_8$-1-NC$_5$H$_5$-10-OEt]$^-$ (**1i**). Indeed, heating EtOH solutions of **8** at reflux demonstrated very slow progress towards a single product over several days. Heating of the reaction mixture at 110 ^{o}C in

a pressure tube for 2 days led to the complete conversion of **8** to the protonated product tentatively assigned as structure **9** and isolated by chromatography in 69% yield (Scheme 3). A more accurate structure for the product might be **1i** with an associated hydronium ion (**1i[H$_3$O]**), which is consistent with the waxy and sticky constitution of the product. Treatment with [Me$_4$N]$^+$OH$^-$•5H$_2$O in MeCN gave **1i[Me$_4$N]**, isolated in 53% yield as orange microcrystals.

Preparation of the morpholine derivative **1j** required a different approach. Since **4[Bu$_4$N]** did not react with morpholine in MeCN solutions, it was reacted with neat morpholine at 85 °C (Scheme 4). The resulting complex mixture of products was reacted with PhI(OAc)$_2$ in AcOH and the bis-zwitterion **6k** was isolated in 30% yield by column chromatography. The subsequent reaction of **6k** with neat pyridine gave the morpholinium derivative **1k** in 76% yield. Deprotonation of the morpholinium group in **1k** with [Et$_4$N]$^+$OH$^-$ in MeCN solutions presumably led to the formation of the desired anion **1j**, which was golden yellow, but unstable under the reaction conditions, and **1j[Et$_4$N]** could not be isolated.

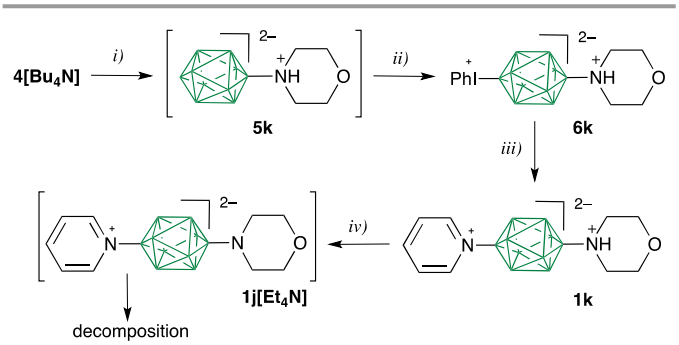

Scheme 4. Preparation of **1k** and attempted deprotonation to **1j**. *Reagents and conditions*: *i*) morpholine 80 °C, 16 h; *ii*) PhI(OAc)$_2$, AcOH/H$_2$O, 0 °C, 1.5 h, 30%; *iii*) pyridine, 80 °C, 16 h, 76%; *iv*) MeCN, used bases: [Et$_4$N]$^+$OH$^-$, LDA, NaH.

The same method was not successful for the preparation of the ethoxy derivative **1i**, and pure phenyliodonium **6i** could not be isolated from complex reaction mixtures.

Derivatives **2[Bu$_4$N]** were obtained by reacting **4[Bu$_4$N]** in neat liquid 4-substituted pyridines (Y = COOEt, Me, OMe) at 80 °C (Scheme 5). For solid 4-cyanopyridine the reaction was conducted in concentrated solutions of **4[Bu$_4$N]** in MeCN (0.55 M) in the presence of 5 eq of the nucleophile.

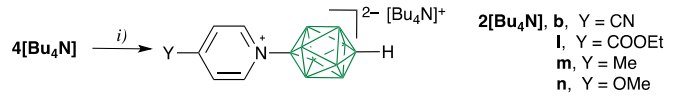

Scheme 5. Preparation of **2[Bu$_4$N]**. *Reagents and conditions*: : *i*) neat pyridine-4-Y for **2l**, **2m**, and **2n**; MeCN and pyridine-4-CN for **2b**, 80 °C, 16 h, 50 – 67% yield.

Finally, ion pair **3[Bu$_4$N]** was prepared using an adaptation of method C shown in Scheme 3. Thus, **2b[Bu$_4$N]** was converted to phenyliodonium derivative **10**, which was solvolyzed in EtOH at 120 °C and the resulting crude protonated product was treated with aqueous [Bu$_4$N]$^+$HSO$_4^-$ and NaHCO$_3$ in CH$_2$Cl$_2$ (Scheme 6). The desired **3[Bu$_4$N]** was isolated by column chromatography passivated with [Bu$_4$N]$^+$HCO$_3^-$ in 22% overall yield based on **2b[Bu$_4$N]**.

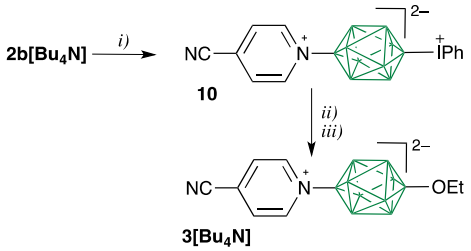

Scheme 6. Preparation of **3[Bu$_4$N]**. *Reagents and conditions*: *i*) PhI(OAc)$_2$, MeCN, r.t., 48 h, 52%; *ii*) EtOH, 120 °C, 24 h; *iii*) [Bu$_4$N]$^+$HSO$_4^-$, NaHCO$_3$, CH$_2$Cl$_2$/H$_2$O, 42% (two steps).

Crystal and molecular structures

Yellow-greenish triclinic crystals of **1b[Et$_4$N]** and **1g[Et$_4$N]** and monoclinic crystals of **1c[Et$_4$N]** and **1k** were obtained from MeCN/EtOH solutions on cooling. Monoclinic crystals of **1d[Bu$_4$N]** and **1e[Et$_4$N]** were grown from MeCN/EtOAc solutions, while **1h** crystallized from EtOH solutions on slow cooling. Orthorhombic crystals of **1f[Et$_4$N]** were obtained by slow evaporation of MeCN/CH$_2$Cl$_2$ solutions. Crystals of **1i[Me$_4$N]** suitable for XRD analysis could not be obtained. Selected bond lengths and angles are collected in Table 1. Molecular structures for all eight new derivatives are shown in Fig. 4.

Crystal systems of most salts **1[R$_4$N]** contain a single ion pair in the asymmetric unit, while **1f[Et$_4$N]** and the previously reported **1a[Et$_4$N]** contain two anions and two cations. The thiocyanato derivative **1f** exhibits positional disorder of the SCN group in both unique molecules. In contrast, the [R$_4$N]$^+$ cation is positionally disordered in most salts with the exception of **1b[Et$_4$N]** and **1e[Et$_4$N]** and **1g[Et$_4$N]**. Additionally, **1g[Et$_4$N]** co-crystallizes with an acetonitrile molecule highly disordered around the special position. Therefore, the solvent molecule was removed from the model using the SQUEEZE tool in PLATON program.[34]

The intracage dimensions of the anions, such as B–B bond distances and angles, are typical for {*closo*-B$_{10}$} derivatives[8, 28, 35] (Table 1). In general, the more electron withdrawing the substituent, the more contracted the {*closo*-B$_{10}$} cage,[35] although there is no linear correlation of the B(1)···B(10) distance with Hammett[36] parameters σ_p.[37] The substituent effect is evident from a comparison of the B(1)···B(10) distance in the parent anion [*closo*-B$_{10}$H$_{10}$]$^{2-}$ (**A**, 3.717(4) Å),[38] monopyridinium **1b–1g** (avg 3.636(14) Å) and bis-zwitterions **1h** (3.620(3) Å) and **1k** (3.611(2) Å). The response to the substituent is largely localized at the substitution apex, which results in contraction of the square pyramid (distance from the equatorial belt). Thus, substitution of the parent anion **A** with pyridinium results in a contraction of the pyramid from 1.100 Å to 1.056 Å in **1a**, which remains nearly constant in the series (Table 1). The pyramid height of the opposite apex is barely affected by substitution with a pyridinium group, but it does respond to the presence of substituent X. For example, the

pyramid height ranges from 1.095 Å for **1a** (X = H) to 1.060 for **1e** (X = I).

Table 1. Selected interatomic distances and angles for derivatives of [*closo*-$B_{10}H_{10}$]$^{2-}$. [a]

	A[Q] [b]	1a[Et_4N] [c,d]	1b[Et_4N]	1c[Et_4N]	1d[Bu_4N]	1e[Et_4N]	1f[Et_4N] [c]	1g[Et_4N]	1h [e]	1k
X	–	H	CN	AcO	N_3	I	SCN	Br	Pyr	MorphH
B(1)–N	–	1.529(3)	1.524(2)	1.530(3)	1.527(2)	1.527(6)	1.528(13)	1.523(2)	1.529(2)	1.523(2)
B(10)–Nu	–	–	1.543(2)	1.462(3)	1.510(2)	2.193(5)	1.879(11)	1.982(2)	1.529(2)	1.547(2)
B(1)–B(2)*	1.701(3)	1.680(5)	1.682(4)	1.681(4)	1.684(5)	1.683(5)	1.681(5)	1.684(7)	1.685(4)	1.677(4)
B(1)···B(2-5) [f]	1.100	1.056	1.052	1.054	1.057	1.058	1.055(5)	1.055	1.056	1.049
B(2)–B(3)*	1.835(9)	1.848(6)	1.856(14)	1.852(7)	1.854(5)	1.851(5)	1.851(15)	1.855(10)	1.857(2)	1.850(7)
B(2)–B(6)*	1.813(6)	1.809(6)	1.8011(6)	1.809(5)	1.808(6)	1.809(10)	1.8010(17)	1.810(4)	1.812(6)	1.809(4)
B(6)–B(7)*	1.835(9)	1.837(7)	1.853(2)	1.846(12)	1.848(5)	1.846(11)	1.851(5)	1.852(5)	1.857(2)	1.846(7)
B(6)–B(10)*	1.701(3)	1.699(6)	1.696(4)	1.698(6)	1.693(5)	1.682(10)	1.685(11)	1.689(5)	1.685(4)	1.679(4)
B(10)···B(6-9) [f]	1.100	1.095	1.077	1.086	1.076	1.060	1.061(1)	1.066	1.056	1.055
B(1)···B(10)	3.717(4)	3.660(4)	3.637(2)	3.647(3)	3.639(2)	3.624(7)	3.619(14)	3.628(3)	3.620(3)	3.611(2)
B–B(1)–N*	130.3(12)	129(2)	128.7(12)	128.8(4)	128.9(16)	129(2)	129.2(12)	128.9(14)	128.8(18)	128.7(18)
B–B(10)–Nu*	130.3(12)	130.1(2)	129(2)	130(5)	129.5(8)	129.1(13)	129(4)	129(2)	128.8(18)	129(3)
Pyr/{B10} [g]	–	24.0/34.0	1.2	14.3	27.8	19.5	4.6/10.8	14.4	21.0/21.0	6.2

[a] Except for unique interatomic distances, all parameters are average values denoted with an asterisk and the esd refers to distribution of individual measurements. [b] Q = 2,6-dimethylpyridinium; treated as D_{4d} symmetric, Ref. [38] [c] 2 molecules. [d] Ref. [18].[e] {*closo*-B_{10}} treated as D_{4d} symmetric. [f] The height of the tetragonal pyramid. [g] Deviation (in °) from the ideal staggered orientation of pyridine.

The pyridine–B(1) distance of 1.527(3) Å is essentially the same in the entire series, within experimental error, for all 9 derivatives. The orientation of the pyridine ring varies from nearly ideally staggered in **1b** to more than half way between staggered and eclipsed (34° off the staggered conformation in **1a**, Table 1). Orientation of the functional groups, OAc, N_3 and SCN is about half way between the staggered and eclipsed conformations, while the morpholinium group adopts a nearly ideal staggered orientation with respect to the {*closo*-B_{10}} cage (7.1° off the ideal staggered).

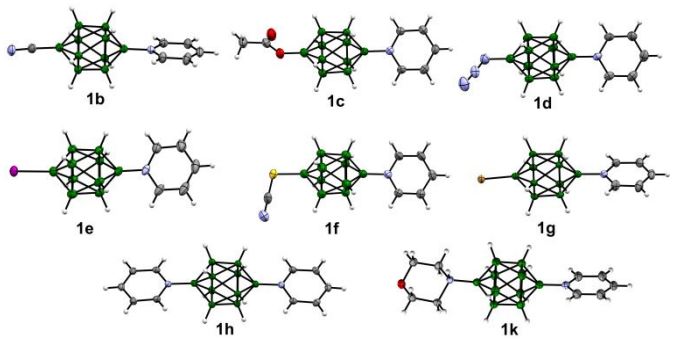

Fig. 4. Atomic displacement ellipsoid representation of **1b–1h** and **1k**. For geometrical dimensions see Table 1 and the text. In **1b–1g** counterions are omitted for clarity and in **1f** only one unique molecule is shown. The corresponding ellipsoids are at the 50% probability level and the numbering system corresponds to the chemical structure.

The B(10)–X distances in derivatives **1** are typical for other derivatives of the [*closo*-$B_{10}H_{10}$]$^{2-}$ anion containing B(1)–CN,[35] B(1)–OCOR,[35] B(1)–I,[33, 39] B(1)–SCN,[40] B(2)–Br,[41] and B(1)–NH_3[42] substituents. The structure of compound **1d** represents the first example of azido derivative of a *closo*-borane. The azido group is nearly linear with the angles $\alpha_{N\text{-}N\text{-}N}$ = 175.6(2)° and $\alpha_{B\text{-}N\text{-}N}$ = 120.9(1)°. Interestingly, the N(1)–N(2) and N(2)–N(3) distances are similar (1.185(2) and 1.154(2) Å, respectively) and much different from those in typical organic azides (*e.g.* 1.229(3) and 1.128(3) Å in 1,6-diazidodiadamantane;[43] 1.242(3) and 1.130(3) Å in 4-Me_2NPhN_3).[44] This is consistent with a shift in negative charge to the terminal nitrogen atom (N3) and significant contribution from the second resonance structure (R–N^-–N^+≡N ⟷ R–N=N^+=N^-).

The supramolecular assembly of the cyano derivative **1b[Et_4N]** appears to be isostructural with that observed in the bromo derivative **1g[Et_4N]** (Fig. 5). The unit cell dimensions *c* are nearly the same for **1b[Et_4N]** and **1g[Et_4N]**, while dimensions *a* and *b* are slightly different in the two structures. The unit cell identity parameter[45] Π = 0.0006 indicates a close resemblance between these two unit cells. Moreover, their crystal structures adopt similar molecular packing. In both of them, molecules of **1b** and **1g** are assembled in infinite chains running along the [100] direction. These chains are stabilized by C–H···B interactions between the pyridine C-H fragment and the boron cluster. The respective intermolecular contacts in **1b[Et_4N]** and **1g[Et_4N]** are 0.337 Å and 0.274 Å shorter than the sum of the van der Waals radii, respectively. Additionally, neighbouring chains are associated through B···C interactions between the boron moiety and the pyridine ring. These contacts for **1b[Et_4N]** and **1g[Et_4N]** are -0.181 Å and -0.127 Å, respectively, inside the van der Waals separation. The resulting double chains running along [100] direction are separated from each other by counterion molecules. Although iodine is regarded as an isomorphous substituent with bromine, the crystal packing of **1e[Et_4N]** is completely different from those observed in **1b[Et_4N]** and **1g[Et_4N]**. In this case the molecular assembly in **1e[Et_4N]** is affected by the presence of the solvent molecule in the crystal lattice.

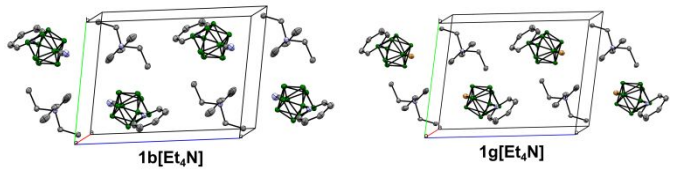

Fig. 5. Packing diagram for **1b[Et$_4$N]** and **1g[Et$_4$N]**. Hydrogen atoms omitted for clarity. Atomic displacement ellipsoid diagram drawn at 50% probability

Molecular modelling

For a better understanding of properties of the investigated compounds, their electronic structures and excitation energies were modelled using the TD-DFT method at the CAM-B3LYP/Def2TZVP // B3LYP/Def2TZVP level of theory in MeCN dielectric medium. Optimizations in series **1** performed with the B3LYP/Def2TZVP method in a weak dielectric medium of PhCl gave accurate molecular geometries, as determined by comparison with selected experimental dimensions: the B(1)···B(10) distance was overestimated by 0.012(4) Å, and B–pyridine and B–X distances were underestimated by –0.006(13) and –0.004(3) Å, respectively.[37] The necessity for inclusion of a weak dielectric medium in geometry optimization of boron zwitterions was demonstrated previously.[35] Other basis sets (*e.g*. TZVP and M06-2x) or lack of dielectric medium give significantly less accurate results.[37]

Photophysical properties

Absorption and emission properties were investigated for all compounds in series **1** and **2** in MeCN solutions, while solvent effects on photophysical properties were studied for the prototypical **1a[Bu$_4$N]**, a representative for both series. Photoluminescent properties in series **1** and **2** were also investigated in the solid state and for two selected derivatives in aggregates.

Solution spectroscopy in MeCN. Electronic absorption spectra measured in MeCN solutions revealed two distinct bands above 200 nm in all compounds in series **1** and **2**: a weak, higher energy band and a broad, medium intensity, lower energy band (Figs. 6 and 7). The former band can be attributed to a π–π* transition in the pyridine ring, since it shows essentially no dependence on substituent X in series **1** and weak dependence on Y in series **2**. In contrast, the position of the lower energy band exhibits a strong substituent dependence in the boron cluster (X in series **1**, Fig. 6, Table 2) and in the pyridine ring (Y in series **2**, Fig. 7). In addition, there is a significant solvatochromic effect (*vide infra*), consistent with assignment as an intramolecular charge transfer (CT) excitation. This assignment is supported with results from TD-DFT calculations: the lowest energy absorption band in **1** and **2** is a (π,π*) excitation involving a transition from the HOMO, localized primarily on the boron cluster, to the LUMO, localized on the pyridinium fragment, as shown for **1b** in Fig. 8.

Analysis of the data in Table 2 indicates that the energy of the CT band decreases in series **1** with decreasing electron-withdrawing character of the substituent X from 3.769 eV for

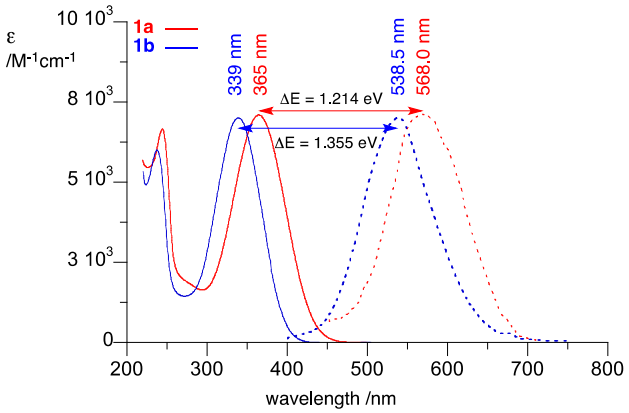

Fig. 6. Electronic absorption (solid line) and normalized emission (dotted line) spectra of **1a[Bu$_4$N]** (red) and **1b[Et$_4$N]** (blue) recorded in MeCN. ΔE is the Stokes shift.

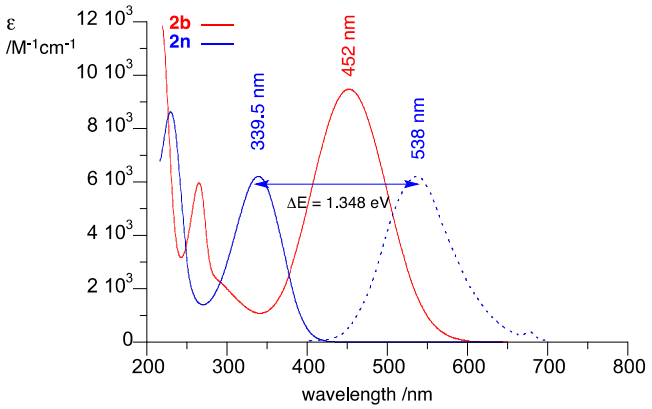

Fig. 7. Electronic absorption (solid line) and normalized emission (dotted line) spectra of **2b[Bu$_4$N]** (red) and **2n[Et$_4$N]** (blue) recorded in MeCN. ΔE is the Stokes shift.

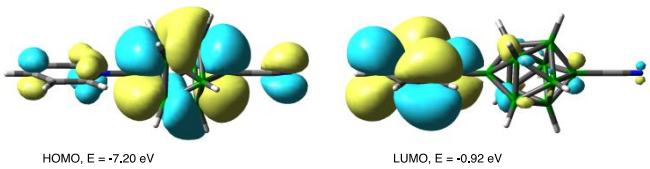

Fig. 8. Contours and energies of molecular orbitals of **1b** relevant to the lowest energy excitation (CAM-B3LYP/Def2TZVP // B3LYP/Def2TZVP level in MeCN dielectric medium).

1k (X=$^+$NHR$_2$) to 3.151 eV for **1i** (X=OEt). Data for **1j** with the most electron-donating NR$_2$ substituent is uncertain due to its chemical instability. In series **2** the substituent effect is opposite and the energy decreases with increasing electron-withdrawing character of the substituent Y from 3.652 eV for **2n** (Y=OMe) to 2.743 eV for **2b** (Y=CN). These results lead to the conclusion that X primarily affects the energy of the HOMO, while Y impacts the energy of the LUMO in derivatives of **1a**.

Finally, anion **3**, which combines the most electron donating substituent X in series **1** and most withdrawing group in series **2** shows an intense absorption at 501.5 nm. This is in agreement with expectations.

Table 2. Experimental and DFT calculated energies of the CT excitation, and emission energies in MeCN solutions and solid state.

	Absorption λ_{max} $\pi\rightarrow\pi^*$		Emission λ_{max} (Stokes Shift)	
	experimental [a] /nm (log ε)	theoretical[b] /nm (*f*)	MeCN sol. [c] /nm (/eV)	solid-state /nm (/eV)
1a	365.0 (3.85) [d]	312.5 (0.291)	568.0 (1.214)	502.5 (0.930)
1b	339.0 (3.85)	295.7 (0.334)	538.5 (1.355)	486.5 (1.109)
1c	368.5 (3.88)	316.1 (0.278)	579.0 (1.223)	513.0 (0.948)
1d	365.0 (3.90)	322.6 (0.328)	536.0 (1.084)	[e]
1e	357.0 (3.92)	305.3 (0.332)	[e]	511.0 (1.047)
1f	344.5 (3.81)	306.6 (0.324)	559 (1.381)	497.0 (1.104)
1g	358.0 (3.91)	306.8 (0.314)	[e]	504.0 (0.999)
1h	335.0 (4.20)	298.8 (0.550)	527.0 (1.348)	471.0 (1.067)
1i	393.5 (3.84)	345.2 (0.293)	[e]	571.5 (0.994)
1j	[f]	370.0 (0.279)	*n/a*	–
1k	329 (3.84)	287.4 (0.323)	530.5 (1.432)	461.0 (1.079)
2b	452.0 (3.98)	390.3 (0.417)	[e]	[e]
2l	431.0 (3.95)	368.5 (0.403)	[e]	[e]
2m	357.5 (3.93)	302.9 (0.336)	550 (1.214)	506.5 (1.020)
2n	339.5 (3.79)	288.4 (0.370)	538.0 (1.348)	467.0 (0.997)
3	501.5 (3.94)	448.8 (0.436)	[e]	[e]

[a] Recorded in MeCN. For full-range absorption spectra see the ESI. [b] Obtained with the TD CAM-B3LYP/Def2TZVP // B3LYP/Def2TZVP method in MeCN dielectric medium. [c] Excitation at the wavelength of maximum absorption. [d] Ref.[18]. [e] No emission. [f] Unreliable data.

Derivatives **1**, except for **1e** (X=I), **1g** (X=Br) and **1i** (X=OEt), and also derivatives **2m** (Y=Me), **2n** (Y=OMe) and **3**, fluoresce weakly in MeCN solutions at substantially lower energies (Table 2, Fig. 6 and 7). The most fluorescent in these series appear to be **1h**, **1k**, **2m** and **2n**, which are structurally similar to pyridinium derivatives that have measured quantum yields of 2-4% in MeCN solutions.[8] In series **1** the Stokes shift increases with increasing electron-withdrawing character of the substituent X from 1.084 eV for **1d** to 1.432 eV for **1k**.

Solvatochromism. To determine the effect of the medium on photophysical processes in series **1** and **2**, absorption and emission spectra were recorded for the parent derivative **1a[Bu$_4$N]**, a representative of both series, in eight solvents covering the full range of polarity.[37] Results shown in Fig. 9 demonstrate a negative solvatochromic effect on the CT and emission bands: the energies increase with increasing polarity of the solvent. Thus, λ_{max} of the CT band decreased from 401.5 nm for THF solution to 338.5 nm for formamide solution (ΔE= 0.575 eV), while the emission spectra changed from 582.0 nm to 542.0 nm in the same solvents (ΔE=0.157 eV). It is notable that the order of solvents effects is not the same for absorption and emission. Also, the Stokes shift diminishes with decreasing solvent polarity from 1.375 eV for formamide to 0.957 eV for THF. These observations are consistent with strong solvation of the anionic S_0 state (GS) and weaker solvent effects on the zwitterionic S_1 state.

Comparison of the experimental excitation energies for **1a[Bu$_4$N]** with solvent E_T30 parameters[46] demonstrates a linear correlation for all data points except for those obtained in CH_2Cl_2 (Fig. 10). The slope of the best-fit line indicates that the solvent affects the electronic absorption of **1a** less than it does the reference pyridinium *N*-phenolate betaine dyes by about 30%. Similar analysis of the emission energy shows poorer correlation with the E_T30 parameters and a significantly smaller solvatochromic effect of about a quarter of that observed for the absorption energies.

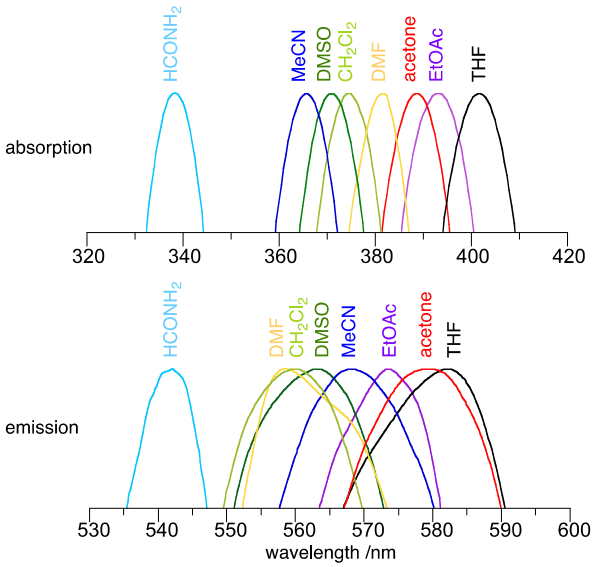

Fig. 9. Normalized absorption (top) and emission (bottom) spectra for **1a[Bu$_4$N]** in selected solvents plotted to show the top of the absorption peak.

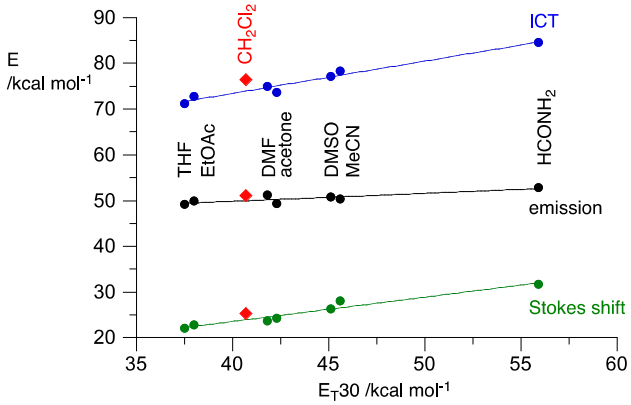

Fig. 10. Correlation of absorption (blue) and emission (black) energies and the Stokes shift (green) for **1a[Bu$_4$N]** with solvent parameter ET30. The best-fit lines (excluding the datapoint for CH_2Cl_2 in red): E_{CT} = 45.2(26)+0.71(6)×E_T30, r^2 = 0.967; E_{em} = 42.9(20)+0.174(45)×E_T30, r^2 = 0.75; E_{Stokes} = 0.584(7)×E_T30, r^2 = 0.943.

Solid-state and aggregation-induced emission (AIE). Most polycrystalline samples of **1** and **2** fluoresce when irradiated with UV light (Table 2). Interestingly, even **1e** and **1g** are photoluminescent in the solid-state despite the presence of a heavy halogen and lack of emission in MeCN solutions. Compound **1i** exhibits solid-state fluorescence at λ_{max} = 572 nm, the lowest energy emission of the series. However, derivative **1d** (X=N_3), which fluoresce, and two pyridinium derivatives, **2b** (Y=CN) and **2l** (Y=COOEt), which do not fluoresce in solution, are not photoluminescent in the solid-

state. The emission energy in the solid state is higher than that in MeCN solutions, as shown for **1b** in Fig. 11. Consequently the Stokes shifts are lower by an average of 0.275(38) eV in all derivatives.

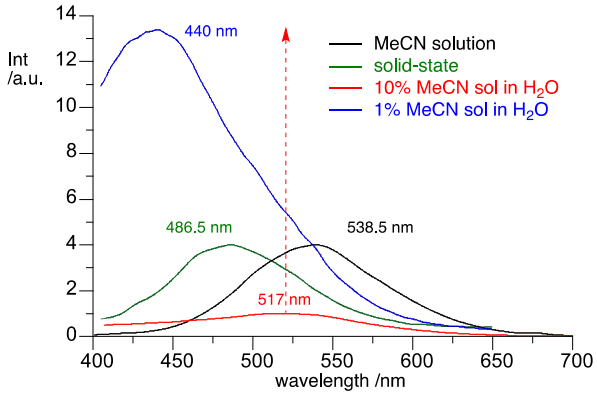

Fig. 11. Emission of **1b** (X=CN) in solution (black), solid-state (green), 10% MeCN solution in H_2O (red) and 1% MeCN solution in H_2O (blue). The intensity in arbitrary units expected for relative 10% (red) and 1% (blue) solutions. The arrow shows a 13 times relative increase.

Finally, aggregation induced emission (AIE) was briefly investigated for two representative derivatives: **1b[Bu$_4$N]** and **1e[Et$_4$N]**. In the former case, a mixture of MeCN solution with H_2O (1:10 ratio) showed emission at 517 nm, which is an intermediate energy between that in MeCN solution (538.5 nm) and that in solid-state (486.5 nm, Fig. 11). In contrast, a 1:100 mixture showed a significant increase in emission intensity (hyperchromic effect) by about 13 times relative to the 1:10 mixture and a marked blue shift (hypsochromic effect) to 440 nm. A similar blue shift of 1:100 and 1:10 mixtures relative to the solid-state emission was observed for **1e[Et$_4$N]**.[37] The observed aggregation and solid-state effects on luminescence (hypso- and hyperchromic shifts of the spectra) are consistent with increasing rigidity of the molecular environment and progressively limited molecular relaxation. This deactivates vibrational relaxation in favour of luminous decay of the excited state. Detailed mechanistic studies have not been performed.

Data analysis. Analysis of experimental photophysical data is enriched by comparison with calculated excitation energies and by correlation analysis with substituent parameters.[36] Hammett σ_p parameters, often used in such analyses, are not available for all substituents X, or they have uncertain values. For the purpose of the present work they were derived from a correlation analysis of ^{1}H NMR data for 20 monosubstituted benzene derivatives Ph–X in acetone-d_6: *N*-morpholinyl (–0.58), acetoxy (0.00), and *N*-morpholinium (0.48).[37] Particularly noteworthy is the revised σ_p value for the OAc group, which is significantly lower than that originally reported,[47] (0.31) and fits the trends for σ_p values for related substituents (*e.g.* σ_p = 0.13 for OCOPh) and other correlations.[35]

Correlation of the substituent effect with the position of the CT band reveals an excellent linear dependence on the σ_p values in both series of derivatives with $r^2 > 0.98$ (Fig. 12). The correlation does not include the data for morpholine derivatives **1j** and **1k** and for **1i** (X = OEt). For anion **1j**, the position of the maximum absorption is uncertain due to its rapid decomposition, while for the bis-zwitterion **1k**, the σ_p value for the morpholinium group derived from the protonated *N*-phenylmorpholine is significantly underestimated (σ_p = 0.48 *vs* σ_p = 0.82 for the $^+$NMe$_3$ group). This is presumably related to the high basicity of the amino group in {*closo*-B$_{10}$} derivatives[48-50] and the lack of dissociation in acetone solutions. In contrast, the reference compound for ^{1}H NMR analysis, the *N*-phenylmorpholinium cation, can exist in equilibrium with the free amine, resulting in a lower-than-expected σ_p value. Using the correlation for the remaining seven data points in series **1**, the expected energy of absorption for **1j** was estimated at 3.13(1) eV (396 nm), which is consistent with a shoulder band in the absorption spectrum of **1j** generated *in situ*.[37] Using the same correlation, the expected value σ_p for the morpholinium group was determined to be 0.92(1), which is reasonable considering the accepted Hammett value of 0.82 for the $^+$NMe$_3$ group[36] and the electron withdrawing character of the oxygen atom in morpholine (*e.g.* σ_p = –0.72 for the NEt$_2$ group and –0.58 for *N*-morpholine).

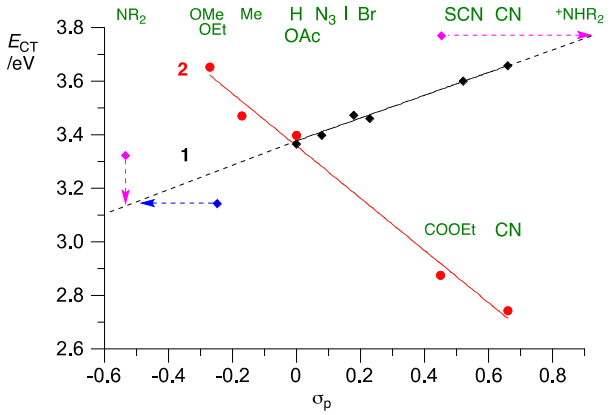

Fig. 12. Hammett correlation of the CT energy in series **1** (black diamonds) and **2** (red dots) with σ_p substituent parameters. The magenta diamonds indicate the data points for morpholine derivatives **1j** and **1k**, and the blue diamond for **1i**. Best-fit functions excluding morpholine and **1i** derivatives: for series **1** (black) E_{CT} = 3.377(9)+0.424(26)×σ_p, r^2 = 0.981 and for series **2** (red) E_{CT} = 3.36(2) – 0.97(6)×σ_p, r^2 = 0.987.

The experimental absorption wavelength for anion **1i** was 15 nm higher than expected from the correlation (Fig. 12). This discrepancy might be due to a different type of interaction of the alkoxy group with the 3-D aromatic {*closo*-B$_{10}$} cluster than with the π-system of benzene, from which the σ_p values were derived. Only one of the two lone pairs of the oxygen atom interacts with the benzene π-system, whereas both unshared electron pairs interact simultaneously with the π-system of the {*closo*-B$_{10}$} cluster (Fig. 13), presumably resulting in the strong

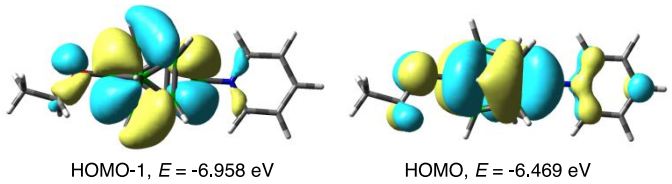

Fig. 13. Contours and energies for two MO of **1i** showing the two lone pairs of the oxygen atom (CAM-B3LYP/Def2TZVP // B3LYP/Def2TZVP level in MeCN dielectric medium).

substituent effect of the OEt group. This conclusion is consistent with the fact that the calculated and experimental (π,π*) CT energies for **1i** fit the trend for other derivatives.

Analysis of the slopes of the two correlation lines in Fig. 12 indicates that the substituent Y (on the pyridine ring) has greater than twice the impact on the excitation energy than substituent X in the boron cluster derivatives of **1a** (slopes 0.97 *vs* 0.42, respectively).

TD-DFT calculations in a MeCN dielectric medium at the CAM-B3LYP/Def2TZVP//B3LYP/Def2TZVP level of theory reproduced the trends in the experimental CT energies in both series of compounds (Fig. 14). The data show better correlation in series **2** (r^2 = 0.999), in which substituent Y is varied on the pyridine ring (slope 1.23±0.02). In contrast, the correlation data for series **1** is somewhat scattered (r^2 = 0.89, slope 1.145±0.006), presumably due to the conformational properties of {*closo*-B_{10}} derivatives. Combined datapoints for both series give a good overall linear correlation with a slope of 1.154(5).

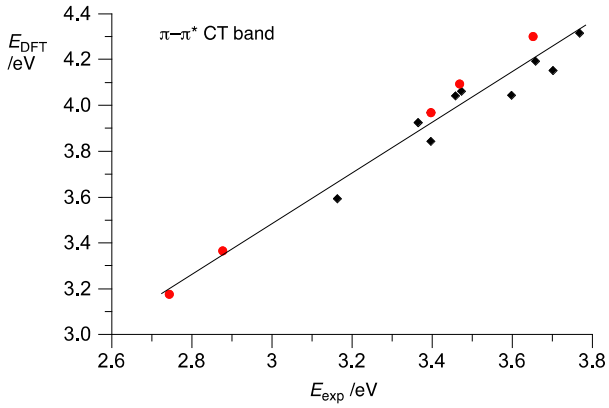

Fig. 14. A comparison of experimental and TD-DFT calculated energy of the CT band in series **1** (black diamonds) and **2** (red dots). Best-fit line for combined datapoints: E_{DFT} = 1.154(5)×E_{exp}, r^2 = 0.955.

Energies of the HOMO and LUMO, the main factors governing the position of the CT band in series **1** and **2**, were correlated with the substituent parameter σ_p (Fig. 15). As might be expected from the less-than-ideal correlation for series **1** in Fig. 14, the relationship of the HOMO energies with σ_p parameter suffers from poor data points for halogen (Br and I), OAc and the parent derivatives (r^2 = 0.854, Fig. 15). Inspection of the FMO energies in series **1** demonstrates that the substituent X affects mainly the energy of the HOMO and the effect is 10 times stronger than that on the LUMO (Fig. 15). This is consistent with the typical distribution of the FMO density in derivatives **1** (Fig. 8), and indicates that the excitation energy in this series is HOMO–controlled. Thus, longer wavelength absorption requires a smaller HOMO–LUMO gap, which is provided with more electron-donating substituents X.

Similar analysis of FMO energy in series **2** shows that substituent Y mainly affects the energy of the LUMO (Fig. 15) and the effect is nearly 14 times stronger than that on the energy of the HOMO. This is again consistent with the FMO distribution in **2**, and shows that the absorption energy in this series is LUMO-controlled. Consequently, a bathochromic shift can be obtained by lowering the LUMO with a strongly electron-withdrawing substituent.

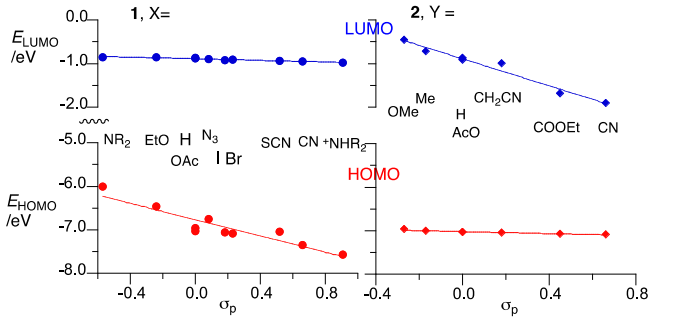

Fig. 15. Correlation of the energy of the HOMO (red) and the LUMO (blue) in series σ_p (left, dots) and **2** (right, diamonds) with substituent parameter σ_p. Best fit lines for series **1**: E_{1HOMO} = -6.77(6) –0.94(14)×σ_p, r^2 = 0.854; E_{1LUMO} = -0.889(4) –0.093(9)×σ_p, r^2 = 0.924; and for series **2**: E_{2HOMO} = -7.023(6) –0.113(18)×σ_p, r^2 = 0.884; E_{2LUMO} = -0.89(4) – 1.56(12)×σ_p, r^2 = 0.969.

Discussion

The present work demonstrates extensive functionalization of the apical position of the [*closo*-$B_{10}H_{10}$]$^{2-}$ anion (**A**) with a diverse set of substituents. Three general approaches to heterodisubstituted derivatives of **A** revealed significant differences in reactivity of aryliodonium intermediates towards nucleophiles. Thus, the presence of an onium substituent in the antipodal position of the {*closo*-B_{10}} cluster increases reactivity towards nucleophilic substitution, presumably through withdrawing of electron density from the iodine center. Consequently, phenyliodonium derivatives **7** and **8** are more reactive than mono-phenyliodonium derivatives **4** and **6**. The latter can be obtained with significant selectivity by monosubstitution of **7** with a more reactive nucleophile.

The order of reactivity revealed in the synthetic work is much different from that expected based on standard nucleophilicity scales.[51] Thus, the observed reactivity towards **4** in MeCN followed the order: N_3^- > CN^- >> pyridine >> amines, OAc^-, Br^-, SCN^- >> EtOH, while the nucleophilicity parameter N follows a different order OAc^- > N_3^- > CN^- > R_2NH > Br^- > SCN^- > pyridine >> EtOH for reactions in MeCN.[51] The surprising lack of reactivity between the phenyliodonium zwitterions of boron clusters and amines was noted previously for derivatives of the [*closo*-1-CB_9H_{10}]$^-$ anion.[22] Thus, the observed reactivity dictates

the method of installation of functional groups in the [*closo*-$B_{10}H_{10}]^{2-}$ anion and the preparation of heterodisubstituted derivatives of **A**.

Using the first method (method A), **4** reacts stoichiometrically with highly reactive nucleophiles (*e.g*. CN^- and N_3^-) and also reacts with an excess (*e.g*. **2b**) or neat (*e.g*. **1a**, **2l–2n**) pyridines to give relatively clean monosubstitution products. On the other hand, thermolysis of **4** in neat morpholine, a secondary amine, gives a complex mixture of products containing about 50% of the expected derivative **5k**. The pure product is isolated as bis-zwitterion **6k**, after installation of the PhI^+ group.

Using the second method (method B) **7** reacts with moderately reactive nucleophiles to substitute one of the two phenyliodonium groups with high selectivity giving **6**. Loss of the onium fragment (PhI^+) deactivates the second phenyliodonium towards substitution. In a variation of this method (method C), the pyridinium substituent is used to activate the phenyliodonium leaving group in **8**, which reacts smoothly with weak nucleophiles including EtOH, giving an alternative approach to series **1**. The process is, however, limited to nucleophiles that do not attack the pyridinium substituents causing ring-opening. The reaction with EtOH is particularly noteworthy. It represents a convenient alternative to the preparation of 1-alkoxy derivatives of anion **A**, which were obtained before from [*closo*-$B_{10}H_9$-1-$N_2]^-$ either by hydroxylation followed by Williamson-type O-alkylation of [*closo*-$B_{10}H_9$-1-OH]$^{2-}$, or attempted direct 1-alkoxylation.[52, 53]

Substitution of the [*closo*-$B_{10}H_{10}]^{2-}$ anion through aryliodonium intermediates can be complicated by several types of side processes. The most important pathway is the formation of B–I instead of B–Nu derivatives through single electron transfer from the Nu^- to the iodine center. The second factor affecting isolation of pure products is the enhanced basicity of the substituents bonded to the {*closo*-B_{10}} cluster, especially those with a heteroatom containing a lone electron pair such as NR_2, OR, N_3, OCOR. In this case, the substituent may undergo spontaneous protonation, *e.g*. during chromatography, and at least partial loss of the $[R_4N]^+$ counterion. For instance, X=OH was recently shown to be a fully protonated oxonium ion.[35] Morpholinium **1k** was fully protonated and all attempts to remove the proton to obtain **1j** resulted in decomposition. Also acetate **1c**, azide **1d** and ethoxide **1i** tend to partially protonate. Protonation can be avoided by treatment with $[R_4N]^+OH^-$ and by using $[R_4N]^+HCO_3^-$ passivated SiO_2 for chromatography. A desirable substituent that is electron-donating but lacks basic centers available for protonation is the alkyl group ($\sigma_p \approx -0.15$),[36] but unfortunately there is currently no synthetic access to alkyl derivatives of the {*closo*-B_{10}} cluster.

Another source of impurities is facile halogenation with electrophiles that may be formed during reactions with $PhI(OAc)_2$, if the solution contains any halide anion (*e.g*. from the $[R_4N]^+X^-$). For example, **11** was identified by XRD analysis as a contaminant in a batch of **1g**, prepared using excess $[Et_4N]^+Br^-$.

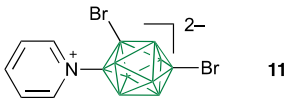

11

Photophysical results demonstrate that the judicious choice of X and Y in the derivatives of [*closo*-$B_{10}H_9$-1-$NC_5H_5]^-$ (**1a**) allows the tuning of the {*closo*-B_{10}} photophysical properties through strategic adjustment of the HOMO and the LUMO energies. While most derivatives **1** and **2** absorb in the range 300–450 nm, pushing the electronic absorption to lower energies requires a strongly electron donating substituent X and a strongly electron withdrawing Y. Among the substituents X, the most electron donating substituent X that gives chemically stable derivatives is ethoxy, while the most electron withdrawing substituent Y reported here is cyano. To test the additivity of substituent effects established for individual series of derivatives, compound **3** was synthesized and characterized (Fig. 16). Using the TD-DFT calculated excitation energy and the correlation in Fig. 14, the predicted electronic absorption in **3** is at λ_{max} = 518±2 nm, which compares favorably to the value observed experimentally (λ_{max} = 501.5 nm). The λ_{max} value is shifted to a lower energy in THF solution, and the predicted maximum of absorption for **3** is 573 nm using the experimental λ_{max} for **3** and the 0.309 eV bathochromic shift observed in **1a** (estimate A in Fig. 16) or at 558±6 nm using λ_{max} for **3** and correlation slope (0.71) in Fig. 10 (estimate B in Fig. 16). The predicted values compare well with the λ_{max} = 560 nm observed for **3** in THF solutions. In formamide, derivative **3** absorbs at 450 nm (predicted 445±6 nm).

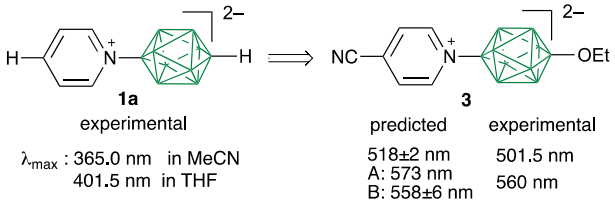

Fig. 16. Predicted effects of substitution of **1a** with X=OEt and Y=CN on absorption spectra and comparison with experimental data for **3**. For details see the text.

Although an alkoxy group appears to be the limit for a substituent effect X to increase the HOMO energy (due to chemical stability), the LUMO presumably could be lowered further by using substituents such as NO_2 (σ_p = 0.78) and SO_2CF_3 (σ_p = 0.98),[36] that are more strongly electron withdrawing than CN (σ_p = 0.66).

Conclusions

The synthetic work reported here has demonstrated that an extensive set of functional groups at the apical position of the [*closo*-$B_{10}H_{10}]^{2-}$anion is accessible through four general approaches and two phenyliodonium zwitterions, **4** and **7**. Structural analysis confirmed the dependence of the {*closo*–B_{10}} cluster geometry on the electronic nature of the apical

substituent, while DFT calculations confirmed the need for a weak dielectric medium for proper geometry optimization.

Spectroscopic investigation of series **1** and **2,** supported with TD-DFT calculations, revealed significant substituent and solvent effects on the position of the (π,π*) CT band in the prototypical chromophore [*closo*-$B_{10}H_9$-1-NC_5H_5]$^-$ (**1a**), which allows the CT absorption band to be tuned in the visible range. Substituents on the pyridine ring (series **2**) affect the LUMO 2.4 times more strongly than substituents on the {*closo*–B_{10}} cluster impact the HOMO (series **1**). The most electron donating substituent that is available to increase the level of the HOMO in chemically stable derivatives of anion **A** is the EtO group, and its effect is significantly stronger than might be expected from the σ_p parameter. Greater latitude in substituent choice is observed in controlling the LUMO. A combination of the EtO and CN (σ_p = 0.66) substituents increased the λ_{max} from 365 nm in **1a** to 501.5 in **3**. Further contraction of the HOMO–LUMO gap to access the low energy range of the visible spectrum is likely possible through more strongly electron withdrawing substituents such as NO_2 (σ_p = 0.78).

About two thirds of the compounds in series **1** and **2** exhibit weak or moderate solution fluorescence, with a smaller substituent impact on the energy range (0.21 eV). Substituents X that quench solution fluorescence of the parent **1a** are halogens (Br, I) or OEt connected directly to the {*closo*–B_{10}} cluster (series **1**), and COOEt and CN groups on the pyridine ring (series **2**). The Stokes shift in these derivatives is substituent-dependent and ranges from 1.084–1.432 eV. Many compounds, even the Br and I derivatives, but not the N_3 derivative, exhibit solid-state emission with a smaller Stokes shift (~1 eV) than solutions. Two selected derivatives containing CN (**1b**) and I (**1e**) substituents, also demonstrated aggregation-induced emission (AIE) in highly dilute MeCN/ H_2O solutions.

The substantial solvatochromic effects observed for **1a** offer additional means to manipulate the position of the absorption band in the range of ΔE=0.575 eV for solvents ranging from THF (E_T30 = 37.5) to formamide (E_T30 = 55.9). The solvatochromic effect for **1a** is about 70% of that observed for the reference pyridinium betaines that define the E_T30 scale. A solvent effect is also observed for emission, although the magnitude is much smaller, about one quarter of that in the absorption spectra. The additivity of the established correlations for series **1** and **2** was demonstrated on anion **3**, which allows the prediction of the CT band energy in other derivatives in selected media.

The results presented here demonstrate synthetic access to a broad range of substituents at the apical position of the [*closo*-$B_{10}H_{10}$]$^{2-}$ anion and describe basic relationships between the structure and photophysical properties of these derivatives. Photophysical effects and behaviour observed in series **1** and **2** demonstrate the potential for the [*closo*-$B_{10}H_{10}$]$^{2-}$ anion to serve as the key building block for a new class of photonic materials with substituent- and medium-tunable intramolecular CT absorption and emission.

Computational Details

Quantum-mechanical calculations were carried out using the Gaussian 09 suite of programs.[54] Geometry optimizations were performed with the B3LYP method[55, 56] and Def2TZVP basis set[57, 58] using tight convergence limits and appropriate symmetry constraints. All calculations were performed in PhCl dielectric medium (arbitrarily chosen) with the PCM model[59] with SCRF (Solvent=C6H5Cl) keyword. The ground state nature of stationary points for the obtained equilibrium geometry was confirmed with vibrational frequency calculations.

Electronic excitation energies for series **1** and **2** and ions **3** in a MeCN dielectric medium were obtained at the CAM-B3LYP/Def2TZVP // B3LYP/Def2TZVP level of theory using the time-dependent DFT method[60] supplied in the Gaussian package. The equilibrium geometry for each compound was obtained in a PhCl dielectric medium (*vide supra*). The solvation model was implemented with the PCM model[59] using the SCRF(solvent=*name*) keyword.

Experimental section

General. Reagents and solvents were obtained commercially. Anion [*closo*-$B_{10}H_{10}$]$^{2-}$ was obtained from $B_{10}H_{14}$ according to a literature procedure.[61] Reactions were conducted in an argon atmosphere and subsequent manipulations in air. TLC analyses were conducted on silica gel plates 60-F254. Column chromatography was performed using 70-230 mesh silica gel (Merck). Melting points were recorded uncorrected in capillary tubes or by DSC. NMR spectra were obtained at 500 MHz (^{1}H), 126 MHz (^{13}C) and 160 MHz (^{11}B) in acetone-d_6 unless specified otherwise. Chemical shifts were referenced to the solvent (acetone-d_6 2.05 ppm for ^{1}H and 29.84 ppm for ^{13}C)[62] and to an external sample of neat BF_3•Et_2O in acetone-d_6 (^{11}B, δ = 0.0 ppm). ^{11}B NMR chemical shifts were taken from the H-decoupled spectra. IR spectra were recorded for neat samples using an ATR attachment. HR mass spectrometry was conducted with the TOF-MS ES method most often in the negative mode.

Preparation of **6[R_4N]** and other intermediates is provided in the ESI.

General procedure for the preparation of [*closo*-$B_{10}H_8$-1-X-10-NC_5H_5]$^-$[R_4N]$^+$ (1[R_4N]).

Method A/B from [closo-$B_{10}H_8$-1-IPh-10-X] (6[R_4N]). Iodonium derivative **6[R_4N]** [37] (typically 0.16 mmol) was dissolved in dry pyridine (1 mL) and heated at 80 °C overnight. Volatiles were removed in vacuum, the semisolid residue was washed with hexanes and then with 5% HCl, dried and then purified by column chromatography (SiO_2, MeCN/CH_2Cl_2) giving the desired product **1[R_4N]** as the first main fraction.

Method C from [closo-$B_{10}H_8$-1-IPh-10-(NC_5H_5)] (8). Iodonium derivative **8** [37] (40 mg, 0.10 mmol) was dissolved in dry MeCN (0.5 mL) appropriate nucleophile salt [R_4N]$^+X^-$ (1.5 eq) was added and the reaction mixture was heated at 80 °C overnight. When EtOH was the nucleophile the reaction was carried out in a pressure tube

at 110 °C for 2 days. Volatiles were removed under vacuum, the semi-solid residue was washed with hexanes and then with dilute HCl (except when EtOH was used), dried and purified by column chromatography (SiO_2, MeCN/CH_2Cl_2) giving the desired product **1[R_4N]** as the first main fraction. The product was further purified by recrystallization, usually from EtOH/CH_2Cl_2.

[*closo*-$B_{10}H_9$-1-NC_5H_5]$^-$ [Bu_4N^+] (1a[Bu_4N]). Starting with **6a** made with method A: 35 mg (50% yield); yellow powder, R_f = 0.2 (MeCN/CH_2Cl_2 1:15): mp 167 °C; ^{1}H NMR (500 MHz, acetone-d_6) δ 0.03–1.22 (m, 8H), 0.97 (t, *J* = 7.4 Hz, 12H), 1.43 (sext, *J* = 7.4 Hz, 8H), 1.76 – 1.85 (m, 8H), 3.34 – 3.51 (m, 8H), 3.88 (br q, *J* = 145.9 Hz, 1H), 7.90 (t, *J* = 7.2 Hz, 2H), 8.35 (tt, J_1 = 7.7 Hz, J_2 = 1.1 Hz 1H), 9.57 (d, *J* = 5.4 Hz, 2H); ^{13}C NMR (126 MHz, acetone-d_6) δ 13.9, 20.4, 24.5, 59.5, 126.5, 141.4, 148.8; ^{11}B NMR (160 MHz, acetone-d_6) δ -27.4 (d, *J* = 135 Hz, 4B), -23.4 (d, *J* = 130 Hz, 4B), 4.7 (d, *J* = 146 Hz, 1B), 13.9 (s, 1B); UV (MeCN) λ_{max} (log ε) 365.0 nm (3.85); IR, *v* 2467 (BH), 1470, 1007, 778, 692 cm^{-1}; HRMS (ESI-) *m/z* calcd. for $C_5H_{14}B_{10}N$: 198.2062, found: 198.2052. Anal. Calcd. for $C_{21}H_{50}B_{10}N_2$: C, 57.49; H, 11.49; N, 6.39. Found: C, 57.70; H, 11.56; N, 6.29.

[*closo*-$B_{10}H_9$-1-NC_5H_5]$^-$ [Cs^+] (1a[Cs]) *via* cation exchange. Dowex-50 ion exchange resin was washed with wet MeOH until the eluent was transparent, and then with small amounts of dry methanol. The resin was used as a stationary phase for ion exchange chromatography for compound **1a[Bu_4N]**. A solution of **1a[Bu_4N]** (1.0 eq) in MeOH/CH_2Cl_2 (5:1) solvent mixture was passed through the short resin pad using methanol. Then CsOH (1.0 eq) was added portionwise and stirred for 10 min. Solvents were removed under reduced pressure and the crude product was washed with water and crystallized from EtOH/CH_2Cl_2 solvent mixture to give pure product: ^{1}H NMR (500 MHz, acetone-d_6) δ 0.13–1.33 (m, 8H), 3.85 (br q, *J* = 145.4 Hz, 1H), 7.90 (t, *J* = 7.2 Hz, 2H), 8.35 (tt, J_1 = 7.9 Hz, J_2 = 1.5 Hz, 1H), 9.57 (d, *J* = 6.5 Hz, 2H); UV (MeCN) λ_{max} 366.0 nm.

[*closo*-$B_{10}H_8$-1-CN-10-NC_5H_5]-[Bu_4N]$^+$ (1b[Bu_4N]). Starting with **6b** made with method B:[37] 56 mg (60% yield) pale yellow-green crystals from MeCN/EtOH; R_f = 0.71 (9% MeCN in CH_2Cl_2); mp 180 °C; ^{1}H NMR (500 MHz, acetone-d_6) *δ* 0.44-1.24 (br m, 8H), 0.97 (t, *J* = 7.4 Hz, 12H), 1.43 (sext, *J* = 7.4 Hz, 8H), 1.81 (quin, *J* = 8.0 Hz, 8H), 3.42 (m, 8H), 7.99 (t, *J* = 7.1 Hz, 2H), 8.45 (t, *J* = 7.7 Hz, 1H), 9.53 (d, *J* = 5.3 Hz, 2H); ^{13}C NMR (126 MHz, acetone-d_6) *δ* 13.9, 20.4, 24.5, 59.5, 127.0, 142.6, 148.7; ^{11}B NMR (160 MHz, acetone-d_6) *δ* -24.5 (d, *J* = 151 Hz, 4B), -23.4 (d, *J* = 142 Hz, 4B), -4.9 (s, 1B), 19.0 (s, 1B); IR *v* 2481 (B-H), 2189 (CN), 1460, 989, 782, 688 cm^{-1}; UV (MeCN) λ_{max} (log ε) 339.0 (3.85); HRMS (ESI-) *m/z* calcd. for $C_6H_{13}B_{10}N_2$: 223.2015, found: 223.2038. Anal. Calcd. for $C_{14}H_{33}B_{10}N_3$: C, 56.98; H, 10.65; N, 9.06. Found: C, 56.90; H, 10.63; N, 8.90.

[*closo*-$B_{10}H_8$-1-OAc-10-NC_5H_5]$^-$ [Et_4N^+] (1c[Et_4N]). The product isolated from column chromatography was washed with a diluted solution of [Et_4N]$^+$OH$^-$. To balance the cation, solutions of **1[R_4N]** in CH_2Cl_2 was washed with an aqueous solution of [R_4N]$^+$OH$^-$ and recrystallized, typically from MeCN/EtOH. Starting with **6c** made with method B:[37] 50 mg (74% yield); pale yellow-green crystals from MeCN/EtOH; R_f = 0.32 (30% MeCN in CH_2Cl_2); mp 253 °C; ^{1}H NMR (500 MHz, acetone-d_6) *δ* 0.44 – 1.10 (br m, 8H), 1.38 (tt, J_1 = 7.2 Hz, J_2 = 1.9 Hz, 12H), 2.31 (s, 3H), 3.48 (q, *J* = 7.3 Hz, 8H), 7.88 – 7.92 (m, 2H), 8.37 (tt, J_1 = 7.7 Hz, J_2 = 1.4 Hz, 1H), 9.57 (d, *J* = 5.3 Hz, 2H); ^{13}C NMR (126 MHz, acetone-d_6) *δ* 7.8, 23.2, 53.1, 126.6, 141.7, 149.3, 172.8; ^{11}B NMR (160 MHz, acetone-d_6) *δ* -28.6 (d, *J* = 127 Hz, 4B), -26.5 (d, *J* = 129 Hz, 4B), 11.3 (s, 1B), 24.0 (s, 1B); IR, *v* 2495 (BH), 1704 (C=O), 1278, 989, 745, 643 cm^{-1}; UV (MeCN) λ_{max} (log ε) 368.5 (3.88); HRMS (ESI-) *m/z* calcd. for $C_7H_{16}B_{10}NO_2$: 256.2117, found: 256.2141. Anal. Calcd. for $C_{15}H_{36}B_{10}N_2O_2$: C, 46.85; H, 9.44; N, 7.28. Found: C, 46.78; H, 9.34; N, 7.17.

[*closo*-$B_{10}H_8$-1-N_3-10-NC_5H_5]$^-$ [Bu_4N]$^+$ (1d[Bu_4N]). Starting with **6d** made with method A:[37] 80 mg (83% yield) or 123.5 mg (64%) overall yield with method B; pale yellow-green crystals from MeCN/EtOAc; R_f = 0.90 (9% MeCN in CH_2Cl_2); mp 156 °C; ^{1}H NMR (500 MHz, acetone-d_6) δ 0.52–1.25 (m, 8H), 0.97 (t, *J* = 7.4 Hz, 12H), 1.43 (sext, *J* = 7.4 Hz, 8H), 1.81 (quin, *J* = 7.7 Hz, 8H), 3.36–3.49 (m, 8H), 7.92 (t, *J* = 7.1 Hz, 2H), 8.39 (t, *J* = 7.7 Hz, 1H), 9.55 (d, *J* = 5.3 Hz, 2H); ^{13}C NMR (126 MHz, acetone-d_6) δ 13.9, 20.4, 24.4, 59.4, 126.7, 141.9, 149.1; ^{11}B NMR (160 MHz, acetone-d_6) δ -27.8 (d, *J* = 132 Hz, 4B), -25.6 (d, *J* = 131 Hz, 4B), 12.0 (s, 1B), 18.4 (s, 1B); IR, *v* 2476 (BH), 2112 (N_3), 1470, 1425, 998, 773, 692 cm^{-1}; UV (MeCN) λ_{max} (log ε) 365.0 (3.90); HRMS (ESI-), calcd. for $C_5H_{13}B_{10}N_4$: *m/z* = 239.2076, found: 239.2048. Anal. Calcd. for $C_{21}H_{49}B_{10}N_5$: C, 52.57; H, 10.30; N, 14.60. Found: C, 52.34; H, 10.16; N, 12.91.

[*closo*-$B_{10}H_8$-1-I-10-NC_5H_5]$^-$ [Bu_4N]$^+$ (1e[Bu_4N]). Method A. Starting with **6e**:[37] 52 mg (46% yield); pale yellow-green crystals from ACN/EtOAc; R_f = 0.93 (9% MeCN in CH_2Cl_2); mp 192 °C; ^{1}H NMR (500 MHz, acetone-d_6) δ 0.40–1.20 (br m, 8H), 0.97 (t, *J* = 7.4 Hz, 12H), 1.43 (sext, *J* = 7.2 Hz, 8H), 1.82 (quin, *J* = 7.9 Hz, 8H), 3.34–3.52 (m, 8H), 7.94 (t, *J* = 6.6 Hz, 2H), 8.42 (td, J_1 = 7.6 Hz, J_2 = 1.1 Hz, 1H), 9.53 (d, *J* = 6.0 Hz, 2H); ^{13}C NMR (126 MHz, acetone-d_6) δ 13.9, 20.4, 24.5, 59.5, 126.8, 142.1, 148.7; ^{11}B NMR (160 MHz, acetone-d_6) δ -23.6 (d, *J* = 94 Hz, 8B), -1.7 (s, 1B), 17.1 (s, 1B); IR, *v* 2467 (BH), 1474, 993, 881, 769, 688 cm^{-1}; UV (MeCN) λ_{max} (log ε) 357.0 (3.92); HRMS (ESI-) *m/z* calcd. for $C_5H_{13}B_{10}NI$: 324.1029, found: 324.1027.

[*closo*-$B_{10}H_8$-1-I-10-NC_5H_5]$^-$ [Et_4N]$^+$ (1e[Et_4N]) *via* cation exchange. Dowex-50 ion exchange resin was freshly washed with wet MeOH until the eluent was transparent, and then with small amounts of dry methanol. The resin was used as a stationary phase for ion exchange chromatography for compound **1e[Bu_4N]**. A solution of **1e[Bu_4N]** (36 mg, 0.064 mmol) in MeOH/CH_2Cl_2 (5:1) solvent mixture was passed through a short resin pad using methanol. Then solution of [Et_4N]$^+$OH$^-$ was added dropwise to the acidic eluent until the solution reached a neutral pH (monitored with pH paper indicator). Solvents were removed under reduced pressure and the crude product was washed with water and crystallized from EtOH/MeCN solvent mixture to give 25 mg (86% yield) of pure product **1e[Et_4N]** as pale-yellow crystals; R_f = 0.33 (9% MeCN in CH_2Cl_2); mp 237 °C. ^{1}H NMR (500 MHz, acetone-d_6) δ 0.37 – 1.29 (br m, 8H), 1.37 (tt, J_1 = 7.2 Hz, J_2 = 1.9 Hz, 12H), 3.46 (q, *J* = 7.2 Hz, 8H), 7.95 (dd, J_1 = 7.7 Hz, J_2 = 6.7 Hz, 2H), 8.43 (tt, J_1 = 7.8 Hz, J_2 = 1.4 Hz, 1H), 9.53 (d, J_1 = 6.5 Hz, J_2 = 1.5 Hz, 2H); ^{13}C NMR (126 MHz, acetone-d_6) δ 7.8, 53.1, 126.8, 142.2, 148.7; ^{11}B NMR (160 MHz, acetone-d_6) δ -23.1 (d, *J* = 96 Hz, 8B), -1.5 (s, 1B), 17.4 (s, 1B); IR, *v*

2476 (BH), 1483, 998, 773, 688 cm^{-1}. Anal. Calcd. for $C_{13}H_{33}B_{10}IN_2$: C, 34.51; H, 7.35; N, 6.19. Found: C, 30.35; H, 6.99; N, 4.04.

[*closo*-$B_{10}H_8$-1-SCN-10-NC_5H_5]$^-$ [Et_4N]$^+$ (1f[Et_4N]). Starting from **6f** made from method B:[37] 59.8 mg (78% yield); Starting from **8** from method C:[37] 21.0 mg (55% yield); pale yellow-green crystals from MeCN/CH_2Cl_2; R_f = 0.42 (9% MeCN in CH_2Cl_2); mp 182 °C; ^{1}H NMR (500 MHz, acetone-d_6) δ 0.31–1.23 (br m, 8H), 1.37 (tt, J_1 = 7.3 Hz, J_2 = 1.9 Hz, 12H), 3.45 (q, J = 7.3 Hz, 8H), 7.98 (dd, J_1 = 7.7 Hz, J_2 = 6.7 Hz, 2H), 8.44 (tt, J_1 = 7.8 Hz, J_2 = 1.5 Hz 1H), 9.53 (dd, J_1 = 6.5 Hz, J_2 = 1.5 Hz, 2H); ^{13}C NMR (126 MHz, acetone-d_6) δ 7.8, 53.2, 119.1, 127.0, 142.6, 148.8; ^{11}B NMR (160 MHz, acetone-d_6) δ -24.3 (d, J = 107 Hz, 4B), -23.9 (d, J = 104 Hz, 4B), 9.2 (s, 1B), 16.6 (s, 1B); IR, v 2481 (BH), 2139 (CN), 1465, 876, 769, 692 cm^{-1}; UV (MeCN) λ_{max} (log ε) 344.5 (3.81); HRMS (ESI-) *m/z* calcd. for $C_6H_{13}B_{10}N_2S$: 255.1735, found: 255.1749. Anal. Calcd. for $C_{14}H_{33}B_{10}SN_3$: C, 43.84; H, 8.67; N, 10.95. Found: C, 43.83; H, 8.54; N, 10.76.

[*closo*-$B_{10}H_8$-1-Br-10-NC_5H_5]$^-$ [Et_4N]$^+$ (1g[Et_4N]). Starting with **6g** made from method B:[37] 61 mg (75% yield); pale yellow-green crystals from MeCN/EtOH; R_f = 0.37 (9% MeCN in CH_2Cl_2); mp 228 °C; ^{1}H NMR (500 MHz, acetone-d_6) δ 0.38 – 1.25 (br m, 8H), 1.38 (tt, J_1 = 7.3 Hz, J_2 = 1.9 Hz, 12H), 3.47 (q, J = 7.3 Hz, 8H), 7.93 (dd, J_1 = 7.7 Hz, J_2 = 6.8 Hz, 2H), 8.41 (tt, J_1 = 7.7 Hz, J_2 = 1.5 Hz, 1H), 9.54 (dd, J_1 = 6.5 Hz, J_2 = 1.5 Hz, 2H); ^{13}C NMR (126 MHz, acetone-d_6) δ 7.8, 53.2, 126.7, 142.0, 148.9; ^{11}B NMR (160 MHz, acetone-d_6) δ -24.8 (d, J = 113 Hz, 4B), -24.2 (d, J = 108 Hz, 4B), 13.7 (s, 1B), 14.3 (s, 1B); IR, v 2481 (BH), 1461, 1002, 778, 692 cm^{-1}; UV (MeCN) λ_{max} (log ε) 358.0 (3.91); HRMS (ESI-) *m/z* calcd. for $C_5H_{13}B_{10}NBr$: 276.1167, found: 276.1207. Anal. Calcd. for $C_{13}H_{33}B_{10}BrN_2$: C, 38.51; H, 8.20; N, 6.91. Found: C, 38.89; H, 7.82; N, 4.24.

[*closo*-$B_{10}H_8$-1,10-2(NC_5H_5)] (1h).[63] A solution of bis-iodonium derivative **7** [32, 37] (100 mg, 0.191 mmol) in dry pyridine (1 mL) was stirred at 80 °C for 12 h. Volatiles were removed in vacuum and the solid residue was washed with EtOH followed by hexane and recrystallized from EtOH to give 21 mg (40% yield) of **1h** as pale yellow crystals; mp 340 °C (DSC; lit.[63] mp 352-353 °C) ^{1}H NMR (500 MHz, acetone-d_6) δ 0.51 – 1.74 (br m, 8H), 8.06 (dd, J_1 = 7.6 Hz, J_2 = 6.7 Hz, 4H), 8.52 (tt, J_1 = 7.9 Hz, J_2 = 1.4 Hz 2H), 9.57 (dd, J_1 = 6.8 Hz, J_2 = 1.3 Hz, 4H); ^{13}C NMR (126 MHz, acetone-d_6) δ 127.3, 143.2, 149.0; ^{11}B NMR (160 MHz, acetone-d_6) δ -24.0 (d, J = 132 Hz, 8B), 18.6 (s, 2B); IR, v 2485 (BH), 1461, 1002, 769, 679 cm^{-1}; UV (MeCN) λ_{max} (log ε) 335.0 (4.20); HRMS (ESI-) *m/z* calcd. for $C_{10}H_{18}B_{10}N_2$: 275.2328, found: 275.2344. Anal. Calcd. for $C_{10}H_{18}B_{10}N_2$: C, 43.78; H, 6.61; N, 10.21. Found: C, 43.70; H, 6.50; N, 10.19.

[*closo*-$B_{10}H_8$-1-OEt-10-NC_5H_5]$^-$[Me_4N]$^+$ (1i[Me_4N]). To a solution of **9** [37] (30.0 mg, 0.124 mmol) in MeCN (1.5 mL), $[Me_4N]^+[OH]^-\bullet 5H_2O$ (22.0 mg, 0.121 mmol, 0.98 eq) was added and the yellow reaction mixture was gently heated until it became orange and homogenous. After stirring for an additional 15 min at room temperature, solvents were removed and the orange residue was washed with cold CH_2Cl_2 to remove traces of impurities to give 20.0 mg (53% yield) of pure **1i[Me_4N]**. Analytically pure product was obtained by recrystallization from an EtOH/MeCN mixture to give orange microcrystals: mp 288 °C; ^{1}H NMR (500 MHz, acetone-d_6) δ 0.14 – 1.10 (br m, 8H), 1.32 (t, J = 7.0 Hz, 3H), 3.44 (s, 12H), 4.12 (m, 2H), 7.82 (dd, J_1 = 6.9 Hz, J_2 = 6.4 Hz, 2H), 8.29 (tt, J_1 = 7.7 Hz, J_2 = 1.2 Hz, 1H), 9.58 (d, J_1 j= 5.6 Hz, 2H); ^{13}C NMR (126 MHz, CD_3CN) δ 18.9, 56.3, 67.5, 126.7, 141.8, 149.5; ^{11}B NMR (160 MHz, acetone-d_6) δ -30.3 (d, J = 133 Hz, 4B), -26.9 (d, J = 131 Hz, 4B), 6.5 (s, 1B), 30.3 (s, 1B); IR, v 2463 (BH), 1484, 1462, 1067, 952, 769, 687 cm^{-1}; UV (MeCN) λ_{max} (log ε) 393.5 (3.84), 247.5 (3.87); HRMS (ESI-) *m/z* calcd. for $C_7H_{19}B_{10}NO$: 243.2403, found: 243.2442. Anal. Calcd. for $C_{11}H_{30}B_{10}N_2O$: C, 42.01; H, 9.62; N, 8.91. Found: C, 41.46; H, 9.28; N, 8.51.

[*closo*-$B_{10}H_8$-1-(NHC_4H_8O)-10-NC_5H_5] (1k). Starting from **5k** made with method A:[37] 43 mg (76% yield); white solid was recrystallized from MeCN/EtOH; R_f = 0.71 (30% MeCN in CH_2Cl_2); mp 317 °C (DSC); ^{1}H NMR (500 MHz, acetone-d_6) δ 0.66 (m, 8H), 3.68 (ddd, J_1 = 13.8, J_2 = 11.4, J_3 = 3.6 Hz, 2H), 3.95 (br d, J = 13.4 Hz, 2H) 4.10 (ddd, J_1 = 12.4 Hz, J_2 = 12.1 Hz, J_3 = 2.0 Hz, 2H), 4.20 (d, J = 12.4 Hz, 2H), 8.02 (t, J = 7.1 Hz, 2H), 8.48 (tt, J_1 = 7.8 Hz, J_2 = 1.3 Hz, 1H), 9.54 (d, J = 5.4 Hz, 2H); ^{13}C NMR (126 MHz, acetone-d_6) δ 56.1, 65.9, 127.1, 143.0, 149.0; ^{11}B NMR (160 MHz, acetone-d_6) δ -27.3 (d, J = 133 Hz, 4B), -25.5 (d, J = 134 Hz, 4B), 17.4 (s, 2B); IR, v 3088 (NH), 2472 (BH), 1461, 1254, 1119, 921, 760, 688 cm^{-1}; UV (MeCN) λ_{max} (log ε) 329.0 (3.84); HRMS (ESI-) *m/z* calcd. for $C_9H_{21}B_{10}N_2O$: 283.2590, found: 283.2597. Anal. Calcd. for $C_9H_{22}B_{10}N_2O$: C, 38.28; H, 7.85; N, 9.92. Found: C, 38.93; H, 7.84; N, 9.64.

Preparation of [*closo*-$B_{10}H_8$-1-(NC_5H_4-4-Y]$^-$[Bu_4N]$^+$ (2[Bu_4N]) from [*closo*-$B_{10}H_8$-1-IPh]$^-$[Bu_4N]$^+$ (4[Bu_4N]). General procedure. A solution of monophenyliodonium derivative **4[Bu_4N]** (60.0 mg, 0.106 mmol) was dissolved in neat 4-substituted pyridine (0.5 mL) and the reaction mixture was stirred overnight at 80 °C. For solid 4-cyanopyridine (55 mg, 5 eq) was used and all reagents were dissolved in small amount of dry MeCN (0.2 mL). Unreacted pyridine was removed under high vacuum and the remaining oily residue was dissolved in CH_2Cl_2 (2 mL) and washed twice with 5% aqueous HCl, then with water. The solvent was evaporated and purified on silica gel (CH_2Cl_2 100% gradient to 10% MeCN in CH_2Cl_2), then recrystallized from EtOH with small amount of CH_2Cl_2 cooled to give pure product in 50 – 67% yield.

[*closo*-$B_{10}H_9$-1-(NC_5H_4-4-CN)]$^-$ [Bu_4N]$^+$ (2b[Bu_4N]). Obtained 26.0 mg (53% yield); Red powder, R_f = 0.2 (MeCN/ CH_2Cl_2 1:15): mp 238 °C; ^{1}H NMR (500 MHz, acetone-d_6) δ 0.07 – 1.18 (br m, 8H), 0.98 (t, J = 7.3 Hz, 12H), 1.44 (sext, J = 7.4 Hz, 8H), 1.83 (quin, J = 8.0 Hz, 8H), 3.29 – 3.56 (m, 8H), 4.14 (br q, J = 145 Hz, 1H), 8.25 (d, J = 6.0 Hz, 2H), 9.75 (d, J = 6.1 Hz, 2H); ^{13}C NMR (126 MHz, acetone-d_6) δ 13.9, 20.4, 24.5, 59.5, 116.5, 123.7, 128.8, 149.6; ^{11}B NMR (160 MHz, acetone-d_6) δ -26.3 (d, J = 132 Hz, 4B), -21.6 (d, J = 128 Hz, 4B), 8.7 (d, J = 145 Hz, 1B), 14.5 (s, 1B); UV (MeCN) λ_{max} (log ε) 452.0 (3.98); IR, v 2467 (BH), 2238 (CN), 1492, 1465, 1420, 998, 863, 742; HRMS (ESI-) *m/z* calcd. for $C_6H_{13}B_{10}N_2$: 223.2015, found: 223.2032. Anal. Calcd. for $C_{22}H_{49}B_{10}N_3$: C, 56.98; H, 10.65; N, 9.06. Found: C, 56.90; H, 10.63; N, 8.90.

[*closo*-$B_{10}H_9$-1-(NC_5H_4-4-COOEt)]$^-$ [Bu_4N]$^+$ (2l[Bu_4N]). Crude product was crystallized from EtOH/CH_2Cl_2 to give 36.0 mg (67% yield) of pure product as a burgundy-red powder, R_f = 0.8 (MeCN/ CH_2Cl_2

1:15); mp 170 °C; ^{1}H NMR (500 MHz, acetone-d_6) δ 0.08 – 1.21 (m, 8H), 0.97 (t, *J* = 7.4 Hz, 12H), 1.43 (sext, *J* = 7.2 Hz, 8H), 1.46 (t, *J* = 7.1 Hz, 3H), 1.81 (quin, *J* = 8.0 Hz, 8H), 3.40 – 3.45 (m, 8H), 4.03 (br q, *J* = 148 Hz, 1H), 4.51 (q, *J* = 7.1 Hz, 2H), 8.31 (d, *J* = 6.8 Hz, 2H), 9.72 (d, *J* = 6.8 Hz, 2H); ^{13}C NMR (126 MHz, acetone-d_6) δ 13.9, 14.4, 20.4, 24.5, 59.5, 63.3, 125.6, 141.3, 149.6, 164.0; ^{11}B NMR (160 MHz, acetone-d_6) δ -26.7 (d, *J* = 131 Hz, 4B), -22.3 (d, *J* = 130 Hz, 4B), 7.1 (d, *J* = 144 Hz, 1B), 14.1 (s, 1B); UV (MeCN) λ_{max} (log ε) 431.0 (3.95); IR, *v* 2467 (BH), 1731 (C=O), 1425, 1285, 1008, 768; HRMS (ESI-) *m/z* calcd. for $C_8H_{18}B_{10}NO_2$: 270.2274, found: 270.2299. Anal. Calcd. for $C_{24}H_{54}B_{10}N_2O_2$: C, 56.43; H, 10.66; N, 5.48. Found: C, 56.48; H, 10.36; N, 5.29.

[*closo*-$B_{10}H_9$-1-(NC_5H_4-4-Me)]$^-$ [Bu_4N]$^+$ (2m[Bu_4N]). Obtained 30.0 mg (63% yield); yellow powder, R_f = 0.2 (MeCN/ CH_2Cl_2 1:15); mp 170 °C; ^{1}H NMR (500 MHz, acetone-d_6) δ 0.04 – 0.90 (m, 8H), 0.97 (t, *J* = 7.4 Hz, 12H), 1.43 (sext, *J* = 7.4 Hz, 8H), 1.81 (quin, *J* = 8.0 Hz, 8H), 2.65 (s, 3H), 3.39 – 3.45 (m, 8H), 3.82 (br q, *J* = 145 Hz, 1H), 7.70 (d, *J* = 6.0 Hz, 2H), 9.38 (d, *J* = 5.9 Hz, 2H); ^{13}C NMR (126 MHz, acetone-d_6) δ 13.9, 20.4, 21.4, 24.56, 59.5, 127.0, 148.0, 154.3; ^{11}B NMR (160 MHz, acetone-d_6) δ -27.7 (d, *J* = 133 Hz, 4B), -23.8 (d, *J* = 129 Hz, 4B), 4.0 (d, *J* = 144 Hz, 1B), 13.7 (s, 1B); UV (MeCN) λ_{max} (log ε) 357.5 (3.93); IR, *v* 2467 (BH), 1488, 1447, 1209, 998, 836; HRMS (ESI-) *m/z* calcd. for $C_6H_{16}B_{10}N$: 212.2219, found: 212.2227. Anal. Calcd. for $C_{22}H_{52}B_{10}N_2$: C, 58.36; H, 11.58; N, 6.19. Found: C, 58.28; H, 11.52; N, 6.00.

[*closo*-$B_{10}H_9$-1-(NC_5H_4-4-OMe)]$^-$ [Bu_4N]$^+$ (2n[Bu_4N]). Obtained 25.0 mg (50% yield); light yellow powder, R_f = 0.2 (MeCN/CH_2Cl_2 1:15); mp 111 °C; ^{1}H NMR (500 MHz, acetone-d_6) δ 0.04 – 1.31 (br m, 8H), 0.97 (t, *J* = 7.4 Hz, 12H), 1.43 (sext, *J* = 7.4 Hz, 8H), 1.81 (quin, *J* = 8.0 Hz, 8H), 3.37 – 3.47 (m, 8H), 3.75 (br q, *J* = 154 Hz, 1H), 4.16 (s, 3H), 7.39 (d, *J* = 7.3 Hz, 2H), 9.33 (d, *J* = 7.3 Hz, 2H); ^{13}C NMR (126 MHz, acetone-d_6) δ 13.9, 20.4, 24.6, 57.5, 59.5, 112.1, 150.1, 169.6; ^{11}B NMR (160 MHz, acetone-d_6) δ -28.0 (d, *J* = 127 Hz, 4B), -24.3 (d, *J* = 125 Hz, 4B), 2.9 (d, *J* = 141 Hz, 1B), 13.7 (s, 1B); UV (MeCN) λ_{max} (log ε) 339.5 (3.79); IR, *v* 2463 (BH), 1631, 1506, 1308, 1196, 1002, 867, 575; HRMS (ESI-) *m/z* calcd. for $C_6H_{16}B_{10}NO$: 228.2168, found: 228.2177. Anal. Calcd. for $C_{22}H_{52}B_{10}N_2O$: C, 56.37; H, 11.18; N, 5.98. Found: C, 56.41; H, 11.19; N, 5.84.

[*closo*-$B_{10}H_8$-1-(EtO)-10-(NC_5H_4-4-CN)]$^-$[Bu_4N]$^+$ (3[Bu_4N]). A suspension of **10** [37] (330 mg, 0.778 mmol) in EtOH (8 mL) was heated in a sealed tube at 120 °C for 24 h with ^{11}B NMR monitoring. The EtOH was removed under high vacuum and the dark red residue was washed with warm hexane (2x) to give a crude product with 80% purity by ^{11}B NMR, which was used for the next step. Attempts at purification using silica gel gave complex mixtures of products containing the partially deprotonated form. ^{1}H NMR (500 MHz, acetone-d_6) δ 0.57 – 1.31 (m, 8H), 1.74 (t, *J* = 7.2 Hz, 3H), 4.88 (q, *J* = 7.3 Hz, 2H), 8.38 (d, *J* = 6.9 Hz, 2H), 9.77 (d, *J* = 6.8 Hz, 2H); ^{11}B NMR (160 MHz, acetone-d_6) δ -27.07 (d, *J* = 136.6 Hz, 4B), -25.08 (d, *J* = 131.3 Hz, 4B), 14.17 (s, 1B), 27.36 (s, 1B). To a portion of the crude product (69.0 mg, ~80% purity) in CH_2Cl_2 (1.5 mL), solid [Bu_4N]$^+$[HSO_4]$^-$ (88 mg, 0.259 mmol) and $NaHCO_3$ (33 mg, 0.389 mmol) were added, followed by a few drops of water. The reaction mixture turned deep purple. After 15 min of stirring, the organic phase was separated, solvents removed and the residue was purified on column chromatography (CH_2Cl_2 gradient to CH_2Cl_2/MeCN 7:1) using SiO_2 gel freshly passivated with [Bu_4N]$^+HCO_3^-$ (see the ESI). Solvents were evaporated to give 55.0 mg (42% yield for 2 steps) of pure **3[Bu_4N]** as a purple solid. Recrystallization produced films or fine powders from combinations of CH_2Cl_2 with Et_2O, or cyclohexane, and EtOH. Mp. 76-78 °C; ^{1}H NMR (500 MHz, acetone-d_6) δ 0.33 – 1.10 (m, 8H), 0.97 (t, *J* = 7.3 Hz, 12H), 1.34 (t, *J* = 6.9 Hz, 3H), 1.43 (sext, *J* = 7.4 Hz, 8H), 1.78 – 1.84 (m, 8H), 3.40 – 3.46 (m, 8H), 4.14 (br s, 2H), 8.14 (d, *J* = 6.8 Hz, 2H), 9.77 (d, *J* = 6.8 Hz, 2H); ^{13}C NMR (126 MHz, acetone-d_6) δ 13.9, 19.0, 20.4, 24.5, 59.5, 67.3, 116.6, 122.8, 128.4, 150.1; ^{11}B NMR (160 MHz, acetone-d_6) δ -28.53 (d, *J* = 127.6 Hz, 4B), -24.38 (d, *J* = 128.7 Hz, 4B), 7.96 (s, 1B), 34.69 (s, 1B); IR, *v* 2467 (BH), 2240 (CN), 1473, 1428, 1212, 1182, 1112, 996, 881cm^{-1}; UV-vis λ_{max} 501.5 nm (log ε = 3.94), 269.5 (log ε = 3.79); HRMS (ESI,-) *m/z* calcd. for $C_8H_{17}B_{10}N_2O$: 267.2277; found: 267.2298. Anal. Calcd. for $C_{24}H_{53}B_{10}N_3O$: C, 56.77; H, 10.52; N, 8.27. Found: C, 56.47; H, 10.36; N, 7.97.

Synthetic details of the intermediates and precursors are available in the ESI.

X-Ray data collection

Single-crystal X-ray diffraction measurements for derivatives **1** were conducted at low temperature (100.0(1) K) using the CuK_α radiation (λ=1.54184 Å). The data was collected and processed using CrysAlisPro program. All structures were solved with the ShelXT[64, 65] structure solution program using Intrinsic Phasing and refined in the ShelXle by the full-matrix least-squares minimization on F^2 with the ShelXL refinement package. All non-hydrogen atoms were refined anisotropically. The C–H and B–H hydrogen atoms were generated geometrically and refined isotropically using a riding model. Full crystallographic data collection and refinement details are provided in the Electronic Supplementary Information (ESI).

CCDC files 1995610-1995617 contain supplementary crystallographic data for this paper. These data can be obtained free of charge from The Cambridge Crystallographic Data Centre via https://www.ccdc.cam.ac.uk/structures/

Electronic spectroscopy

Electronic absorption spectra were measured for 3 concentrations in spectrophotometric grade MeCN and molar extinction coefficients ε were obtained from the Beer's Law plot with typical r^2 of >0.99 for each compound. Solvatochromic studies of **1a** were conducted similarly recording spectra for a single dilute solution.

Fluorescence spectra were recorded for diluted MeCN solutions using a Hitachi F-4500 Fluorescence Spectrophotometer. The excitation wavelength was set to the absorbance max and λ_{em} was scanned from λ_{max} +50 nm to 900 nm. Relative intensity and λ_{em} of fluorescence were somewhat concentration-dependent in weakly fluorescent compounds.

Solid-state fluorescence was measured for polycrystalline samples in a borosilicate glass capillary. The sample was excited at the wavelength on maximum absorption obtained in MeCN solutions. The normalized emission spectra are shown in ESI.

For AIE measurements, aliquots of a 2.45 x 10^{-4} M solution of **1b[Bu$_4$N]** in MeCN and a 1.22 x 10^{-4} M solution of **1e[Et$_4$N]** in MeCN were added to 3.0 mL distilled water in a quartz cuvette and mixed by pipette. Solutions of 1%, 9.1%, and 16.7% of MeCN in H_2O were prepared from the addition of 30, 300, and 600 μL of stock solution, respectively, to 3.0 mL of H_2O. The resulting concentrations of **1b[Bu$_4$N]** were: 8.09 x 10^{-5} M (1%), 2.23×10^{-5} M (9.1%), 4.08×10^{-5} M (16.7%). The excitation wavelength was set to the absorbance λ_{max} and λ_{em} was scanned from λ_{max} +50 nm to 900 nm. Selected data are collected in Table 2 and all spectra and details of data analysis are shown in the ESI.

Conflicts of interest

There are no conflicts to declare.

Acknowledgements

This work was supported by the National Science Foundation (DMR-1611250 and XRD facility CHE-1626549 grants) and Foundation for Polish Science (TEAM/2016-3/24). We thank Muhammad O. Ali for technical assistance.

Notes and references

1. R. Núñez, M. Tarrés, A. Ferrer-Ugalde, F. Fabrizi de Biani and F. Teixidor, Electrochemistry and photoluminescence of icosahedral carboranes, boranes, metallacarboranes, and their derivatives, *Chem. Rev.*, 2016, **116**, 14307-14378.
2. P. A. Jelliss Photoluminescence from boron-based polyhedral clusters in *Boron Science: New Technologies and Applications*, N. S. Hosmane, Ed.; CRS Press, Nw York 2012, pp 355-384.
3. J. Ochi, K. Tanaka and Y. Chujo, Recent progress in the development of solid-state luminescent *o*-carboranes with stimuli responsivity, *Angew. Chem. Int. Ed.*, 2020, **59**, 9841–9855.
4. S. Mukherjee and P. Thilagar, Boron clusters in luminescent materials *Chem. Commun.*, 2016, **52**, 1070-1093.
5. K.-R. Wee, Y.-J. Cho, S. Jeong, S. Kwon, J.-D. Lee, I.-H. Suh and S. O. Kang, Carborane-based optoelectronically active organic molecules: Wide band gap host materials for blue phosphorescence, *J. Am. Chem. Soc.*, 2012, **134**, 17982–17990.
6. D. M. Murphy, D. M. P. Mingos, J. L. Haggitt, H. R. Powell, S. A. Westcott, T. B. Marder, N. J. Taylor and D. R. Kanis, Synthesis of icosahedral carboranes for second-harmonic generation. Part 2, *J. Mater. Chem.*, 1993, **3**, 139-148.
7. R. Hamasaki, M. Ito, M. Lamrani, M. Mitsuishi, T. Myashita and Y. Yamamoto, Nonlinear optical studies of fullerene–arylethyne hybrids, *J. Mater. Chem.*, 2003, **13**, 21-26.
8. A. Jankowiak, A. Baliński, J. E. Harvey, K. Mason, A. Januszko, P. Kaszyński, V. G. Young, Jr. and A. Persoons, [*closo*-$B_{10}H_{10}$]$^{2-}$ as a structural element for quadrupolar liquid crystals: A new class of liquid crystalline NLO chromophores, *J. Mater. Chem. C*, 2013, **1**, 1144-1159.
9. J. Abe, N. Nemoto, Y. Nagase, Y. Shirai and T. Iyoda, A new class of carborane compounds for second-order nonlinear optics: Ab initio molecular orbital study of hyperpolarizabilities for 1-(1′,X′-dicarba-*closo*-dodecaborane-1′-yl)-*closo*-dodecaborate dianion (X = 2, 7, 12), *Inorg. Chem.*, 1998, **37**, 172-173.
10. K. Base, M. T. Tierney, A. Fort, J. Muller and M. W. Grinstaff, On the second-order nonlinear optical structure-property relationships of metal chromophores, *Inorg. Chem.*, 1999, **38**, 287-289.
11. D. G. Allis and J. T. Spencer, Polyhedral-based nonlinear optical materials. 2. Theoretical investigation of some new high nonlinear optical response compounds involving polyhedral bridges with charged aromatic donors and acceptors, *Inorg. Chem.*, 2001, **40**, 3373-3380.
12. J. Taylor, J. Caruso, A. Newlon, U. Englich, K. Ruhlandt-Senge and J. T. Spencer, Polyhedral-based nonlinear optical materials. 3. Synthetic studies of cyclopentadiene- and cycloheptatriene-substituted polyhedral compounds: Synthesis of 1,12-[(C_7H_7)$C_2B_{10}H_{10}$($C_5H_3Me_2$)] and related species, *Inorg. Chem.*, 2001, **40**, 3381-3388.
13. B. Grüner, Z. Janoušek, B. T. King, J. N. Woodford, C. H. Wang, V. Všetečka and J. Michl, Synthesis of 12-substituted 1-carba-*closo*-dodecaborate anions and first hyperpolarizability of the 12-$C_7H_6^+$-$CB_{11}H_{11}^-$ Ylide, *J. Am. Chem. Soc.*, 1999, **121**, 3122–3126.
14. A. Miniewicz, A. Samoc, M. Samoc and P. Kaszynski, Observation of second-harmonic generation in an oriented glassy nematic phase of a *closo*-decaborane derivative, *J. Appl. Phys.*, 2007, **102**, 033108.
15. A. Vöge and D. Gabel, Boron derivatives for application in nonlinear optics in *Boron Science: New Technologies and Applications*, N. S. Hosmane, Ed.; CRS Press, Nw York 2012, pp 295-317.
16. D. Tu, S. Cai, C. Fernandez, H. Ma, X. Wang, H. Wang, C. Ma, H. Yan, C. Lu and Z. An, Boron-cluster-enhanced ultralong organic phosphorescence, *Angew. Chem. Int. Ed.*, 2019, **58**, 9129-9133.
17. K. M. Harmon, A. B. Harmon and A. A. MacDonald, Ionic organoboranes. IV. Preparation and properties of the $C_7H_6B_{10}H_9^-$ and $C_7H_6B_{12}H_{11}^-$ hemiousenide ions, *J. Am. Chem. Soc.*, 1969, **91**, 323-329.
18. P. Tokarz, P. Kaszyński, S. Domagała and K. Woźniak, The [*closo*-$B_{12}H_{11}$-1-IAr]$^-$ zwitterion as a precursor to monosubstituted derivatives of [*closo*-$B_{12}H_{12}$]$^{2-}$, *J. Organometal. Chem.*, 2015, **798**, 70-79.
19. M. O. Ali, J. C. Lasseter, R. Żurawiński, A. Pietrzak, J. Pecyna, J. Wojciechowski, A. C. Friedli, D. Pociecha and P. Kaszyński, Thermal and photophysical properties of highly quadrupolar liquid crystalline derivatives of the [*closo*-$B_{12}H_{12}$]$^{2-}$ anion, *Chem. Eur. J.*, 2019, **25**, 2616-2630.
20. J. Pecyna, B. Ringstrand, S. Domagała, P. Kaszyński and K. Woźniak, Synthesis and characterization of 12-pyridinium derivatives of the [*closo*-1-$CB_{11}H_{12}$]$^-$ anion, *Inorg. Chem.*, 2014, **53**, 12617-12626.
21. J. Pecyna, D. Pociecha and P. Kaszyński, Zwitterionic pyridinium derivatives of [*closo*-1-CB_9H_{10}]$^-$ and [*closo*-1-$CB_{11}H_{12}$]$^-$ as high Δε additives to a nematic host, *J. Mater. Chem. C*, 2014, **2**, 1585-1591.
22. R. Żurawiński, R. Jakubowski, S. Domagała, P. Kaszyński and K. Woźniak, Regioselective functionalization of the

[*closo*-1-CB_9H_{10}]$^-$ anion through iodonium zwitterions, *Inorg. Chem.*, 2018, **57**, 10442-10456.

23. B. Ringstrand, P. Kaszynski and A. Franken, Synthesis and reactivity of [*closo*-1-CB_9H_9-1-N_2]: Functional group interconversion at the carbon vertex of the {*closo*-1-CB_9} cluster, *Inorg. Chem.*, 2009, **48**, 7313-7329.
24. A. B. Harmon and K. M. Harmon, Ionic organoboranes. II. Cesium tropenylium undecahydroclovododecaborate. Cage-ring interactions in $C_7H_6B_{10}H_9^-$ and $C_7H_6B_{12}H_{11}^-$ ions, *J. Am. Chem. Soc.*, 1966, **88**, 4093-4094.
25. K. M. Harmon and S. H. Gill, Carbonium ion salts. Part 16. Molecular orbital study of tropylium ions with borane anion and carborane substituents (hemiousene compounds), *J. Mol. Struct.*, 2002, **607**, 181-188.
26. P. Kaszynski, J. Huang, G. S. Jenkins, K. A. Bairamov and D. Lipiak, Boron clusters in liquid crystals, *Mol. Cryst. Liq. Cryst.*, 1995, **260**, 315-332.
27. I. B. Sivaev, A. V. Prikaznov and D. Naoufal, Fifty years of the *closo*-decaborate anion chemistry, *Collect. Czech. Chem. Commun.*, 2010, **75**, 1149-1199.
28. K. Y. Zhizhin, A. P. Zhdanov and N. T. Kuznetsov, Derivatives of *closo*-decaborate anion $[B_{10}H_{10}]^{2-}$ with *exo*-polyhedral substituents *Russ. J. Inorg. Chem.*, 2010, **55**, 2089-2127.
29. S. Pakhomov, P. Kaszynski and V. G. Young, Jr., 10-Vertex *closo*-boranes as potential π linkers for electronic materials, *Inorg. Chem.*, 2000, **39**, 2243-2245.
30. P. Kaszynski, S. Pakhomov and V. G. Young, Jr., Investigation of electronic interactions between *closo*-boranes and their triple-bonded substituents, *Collect. Czech. Chem. Commun.*, 2002, **67**, 1061-1083.
31. P. Kaszynski, in *Anisotropic Organic Materials-Approaches to Polar Order*, eds. R. Glaser and P. Kaszynski, ACS Symposium Series, Washington, D.C., 2001, vol. 798, pp. 68-82.
32. P. Kaszynski and B. Ringstrand, Functinalization of boron clusters *via* iodonium zwitterions, *Angew. Chem. Int. Ed.*, 2015, **54**, 6576-6581.
33. E. Rzeszotarska, I. Novozhilova and P. Kaszyński, Convenient synthesis of [*closo*-$B_{10}H_9$-1-I]$^{2-}$ and [*closo*-$B_{10}H_8$-1,10-2I]$^{2-}$ anions, *Inorg. Chem.*, 2017, **56**, 14351-14356.
34. A. L. Spek, Single-crystal structure validation with the program *PLATON*, *J. Appl. Cryst.*, 2003, **36**, 7-13.
35. L. Jacob, E. Rzeszotarska, A. Pietrzak, V. G. Young, Jr. and P. Kaszyński, Synthesis, structural analysis, and functional group interconversion in the [*closo*-$B_{10}H_8$-1,10-2X]$^{2-}$ (X = CN, $[OCRNMe_2]^+$, OCOR, and $[OH_2]^+$) derivatives, *Eur. J. Inorg. Chem.*, 2020, 3083-3093.
36. C. Hansch, A. Leo and R. W. Taft, A survey of Hammett substituent constants and resonance and field parameters, *Chem. Rev.*, 1991, **91**, 165-195.
37. For details see the ESI.
38. S. Mebs, R. Kalinowski, S. Grabowsky, D. Förster, R. Kickbusch, E. Justus, W. Morgenroth, C. Paulmann, P. Luger, D. Gabel and D. Lentz, Real-space indicators for chemical bonding. Experimental and theoretical electron density studies of four deltahedral boranes, *Inorg. Chem.*, 2011, **50**, 90-103.
39. C. Nachtigal and W. Preetz, Dipyridiniomethane 1-iodo-*closo*-decaborate, $[(C_5H_5N)_2CH_2][1\text{-}IB_{10}H_9]$, *Acta Cryst. Sect. C*, 1996, **52**, 453.
40. C. Nachtigal and W. Preetz, Kristallstrukturen von $(PPh_4)_2$[1-(SCN)$B_{10}H_9$] und $(AsPh_4)_2$[1,10-$(SCN)_2B_{10}H_8$] *Z. Anorg. Allg. Chem.*, 1997, **623**, 347-350.
41. W. Preetz and C. Nachtigal, Kristallstruktur von dipyridiniomethan-monohalogenohydro-*closo*-decaboraten(2-), $[(C_5H_5N)_2CH_2][2\text{-}XB_{10}H_9]$; X = Cl, Br, I, *Z. Anorg. Allg. Chem.*, 1995, **621**, 1632-1636.
42. C. Nachtigal, O. Haeckel and W. Preetz, Darstellung und kristallstrukturen von [P(C_6H_5)[1-$(NH_3)B_{10}H_9$] und $Cs[(NH_3)B_{12}H_{11}]\bullet 2CH_3OH$, *Z. Anorg. Allg. Chem.*, 1997, **623**, 1385-1388.
43. M. Šekutor, K. Molčanov, L. Cao, L. Isaacs, R. Glaser and K. Mlinarić-Majerski, Design, synthesis, and X-ray structural analyses of diamantane diammonium salts: Guests for cucurbit[*n*]uril (CB[*n*]) hosts, *Eur. J. Org. Chem.*, 2014, 2533-2542.
44. A. Schulz, M. Thomas and A. Alexander Villinger, Tetrazastannoles *versus* distannadiazanes – a question of the tin(II) source, *Dalton Trans.*, 2019, **48**, 125-132
45. A. Kálmán, L. Párkányi and G. Argay, Classification of the isostructurality of organic molecules in the crystalline state, *Acta Cryst., Sect. B*, 1993, **49**, 1039-1049.
46. J. P. Cerón-Carrasco, D. Jacquemin, C. Laurence, A. Planchat, C. Reichardt and K. Sraïdi, Solvent polarity scales: determination of new ET(30) values for 84 organic solvents, *J. Phys. Org. Chem.*, 2014, **27**, 512-518.
47. D. H. McDaniel and H. C. Brown, An extended table of Hammett substitutent constants based on the ionization of substituted benzoic acids, *J. Org. Chem.*, 1958, **23**, 420-427.
48. W. R. Hertler and M. S. Raasch, Chemistry of boranes. XIV. Amination of $B_{10}H_{10}^{-2}$ and $B_{12}H_{12}^{-2}$ with hydroxylamine-*O*-sulfonic Acid, *J. Am. Chem. Soc.*, 1964, **86**, 3661-3668.
49. W. H. Knoth, H. C. Miller, D. C. England, G. W. Parshall and E. L. Muettertiese, Derivative chemistry of $B_{10}H_{10}^{2-}$ and $B_{12}H_{12}^{2-}$, *J. Am. Chem. Soc.*, 1962, **84**, 1056-1057.
50. B. Ringstrand, P. Kaszynski, V. G. Young, Jr. and Z. Janoušek, The anionic amino acid [*closo*-1-CB_9H_8-1-COO-10-NH_3]$^-$ and dinitrogen acid [*closo*-1-CB_9H_8-1-COOH-10-N_2] as key precursors to advanced materials: Synthesis and reactivity, *Inorg. Chem.*, 2010, **49**, 1166-1179.
51. Mayr's Database Of Reactivity Parameters, https://www.cup.lmu.de/oc/mayr/reaktionsdatenbank/
52. A. V. Prikaznov, V. I. Bragin, M. N. Davydova, I. B. Sivaev and V. I. Bregadze, Synthesis of alkoxy derivatives of decahydro-*closo*-decaborate anion, *Collect. Czech. Chem. Commun.*, 2007, **72**, 1689-1696.
53. V. I. Bragin, I. B. Sivaev, V. I. Bregadze and N. A. Votinova, Synthesis of the 1-hydroxy-*closo*-decaborate anion [1-$B_{10}H_9OH]^{2-}$, *J. Organometal. Chem.*, 2005, **690**, 2847-2849.
54. Frisch, M. J. *et al* Gaussian 09, Revision C.01, Gaussian, Inc., Wallingford CT, 2011.
55. A. D. Becke, Density-functional thermochemistry. III. The role of exact exchange, *J. Chem. Phys.*, 1993, **98**, 5648-5652.
56. C. Lee, W. Yang and R. G. Parr, Development of the Colle-Salvetti correlation-energy formula into a functional of the electron density, *Phys. Rev. B,*, 1988, **37**, 785-789.
57. F. Weigend, Accurate Coulomb-fitting basis sets for H to Rn, *Phys. Chem. Chem. Phys.*, 2006, **8**, 1057-1065.

58. F. Weigend and R. Ahlrichs, Balanced basis sets of split valence, triple zeta valence and quadruple zeta valence quality for H to Rn: Design and assessment of accuracy, *Phys. Chem. Chem. Phys.*, 2005, **7**, 3297-3305.
59. M. Cossi, G. Scalmani, N. Rega and V. Barone, New developments in the polarizable continuum model for quantum mechanical and classical calculations on molecules in solution, *J. Chem. Phys.*, 2002, **117**, 43-54, and references therein.
60. R. E. Stratmann, G. E. Scuseria and M. J. Frisch, An efficient implementation of time-dependent density-functional theory for the calculation of excitation energies of large molecules, *J. Chem. Phys.*, 1998, **109**, 8218-8224.
61. M. F. Hawthorne, R. L. Pilling and W. H. Knoth, Bis(triethylammonium) decahydrodecaborate(2-), *Inorg. Synth.*, 1967, **9**, 16–19.
62. G. R. Fulmer, A. J. M. Miller, N. H. Sherden, H. E. Gottlieb, A. Nudelman, B. M. Stoltz, J. E. Bercaw and K. I. Goldberg, NMR chemical shifts of trace impurities: Common laboratory solvents, organics, and gases in deuterated solvents relevant to the organometallic chemist, *Organometallics*, 2010, **29**, 2176–2179.
63. W. H. Knoth, Chemistry of boranes. XXVI. Inner diazonium salts 1,10-$B_{10}H_8(N_2)_2$ -$B_{10}Cl_8(N_2)_2$, and -$B_{10}I_8(N_2)_2$, *J. Am. Chem. Soc.*, 1966, **88**, 935-939.
64. G. M. Sheldrick, *SHELXT* – Integrated space-group and crystal- structure determination, *Acta Cryst., Sect. A*, 2015, **A71**, 3-8.
65. G. M. Sheldrick, Crystal structure refinement with *SHELXL*, *Acta Cryst., Sect. C*, 2015, **C71**, 3-8.

Graphical TOC

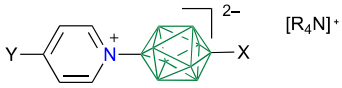

X = H, CN, OAc, N_3, I, SCN, Br, Pyridine, EtO, morpholine
Y = H, CN, COOEt, Me, OMe

THF MeCN formamide